Endosomal cargo recycling mediated by Gpa1 and phosphatidylinositol 3-kinase is inhibited by glucose starvation

Kamilla M. E. Laidlaw[a,†], Katherine M. Paine[a,†], Daniel D. Bisinski[a,‡], Grant Calder[b], Karen Hogg[b], Sophia Ahmed[b], Sally James[b], Peter J. O'Toole[b], and Chris MacDonald[a,*]
[a]York Biomedical Research Institute and Department of Biology and [b]Bioscience Technology Facility, Department of Biology, University of York, YO10 5DD York, UK

ABSTRACT Cell surface protein trafficking is regulated in response to nutrient availability, with multiple pathways directing surface membrane proteins to the lysosome for degradation in response to suboptimal extracellular nutrients. Internalized protein and lipid cargoes recycle back to the surface efficiently in glucose-replete conditions, but this trafficking is attenuated following glucose starvation. We find that cells with either reduced or hyperactive phosphatidylinositol 3-kinase (PI3K) activity are defective for endosome to surface recycling. Furthermore, we find that the yeast Gα subunit Gpa1, an endosomal PI3K effector, is required for surface recycling of cargoes. Following glucose starvation, mRNA and protein levels of a distinct Gα subunit Gpa2 are elevated following nuclear translocation of Mig1, which inhibits recycling of various cargoes. As Gpa1 and Gpa2 interact at the surface where Gpa2 concentrates during glucose starvation, we propose that this disrupts PI3K activity required for recycling, potentially diverting Gpa1 to the surface and interfering with its endosomal role in recycling. In support of this model, glucose starvation and overexpression of Gpa2 alter PI3K endosomal phosphoinositide production. Glucose deprivation therefore triggers a survival mechanism to increase retention of surface cargoes in endosomes and promote their lysosomal degradation.

INTRODUCTION

The surface localization and activity of plasma membrane (PM) proteins can be regulated by the balance of action between endocytic trafficking pathways. Clathrin-dependent and -independent mechanisms internalize proteins from the PM, which then transit through different compartments en route to the lysosome for degradation. Various recycling mechanisms transport cargoes back to the surface, providing multiple regulatable steps to fine-tune the surface protein environment in response to external conditions. Yeast has been a useful model organism to uncover conserved trafficking mechanisms of surface proteins. Upon internalization from the yeast PM, surface cargoes can be sorted to the lysosome-like vacuole, in a process that involves cargo ubiquitination, mediated by E1-E2-E3 enzyme cascade in collaboration with competing trafficking adaptors (MacDonald *et al.*, 2020; Sardana and Emr, 2021). Ubiquitinated cargoes are recognized at multivesicular bodies (MVBs) by the endosomal sorting complex required for transport (ESCRT) apparatus, which also package cargo destined for degradation into intraluminal vesicles (Laidlaw and MacDonald, 2018). Proteins that are not targeted for degradation can recycle back to the surface, including a retrograde route that traffics material to the surface via the *trans*-Golgi network (TGN) using dedicated machineries that interact with recycled cargoes (Chen *et al.*, 2019). Recycling in animal cells can also occur directly from

early endosomes or indirectly, first traversing defined recycling endosomes (MacDonald and Piper, 2016). Endosomal organization and recycling mechanisms in yeast are less clear (Ma and Burd, 2020), but work using the yeast exocytic v-SNARE protein Snc1 revealed that multiple endosomal transport steps regulate Snc1 trafficking back to the PM (Ma *et al.*, 2017; Ma and Burd, 2019; Best *et al.*, 2020). Although retrograde recycling is perturbed by deubiquitination (Xu *et al.*, 2017), recycling of some nutrient transporters is triggered by deubiquitination (MacDonald and Piper, 2017; Laidlaw *et al.*, 2021). Genetic dissection of the latter pathway implies that recycling is controlled at transcriptional and metabolic levels (MacDonald and Piper, 2017; Amoiradaki *et al.*, 2021), suggesting that early endocytic trafficking decisions contribute to the eventual down-regulation of surface cargoes in response to nutritional cues.

During periods of nutritional stress, multiple mechanisms involving surface cargoes and endocytic pathways are modulated to promote proliferation, particularly in cancer cells (Selwan *et al.*, 2016; Finicle *et al.*, 2018). Recycling internalized cargoes back to the surface can promote anabolic processes. During starvation, when some such processes are not required, reduced recycling can route surface cargoes to the lysosomal (vacuolar in yeast) degradation pathway instead, to promote catabolism. Conceptually, these pathways can be modulated to drive growth/proliferation appropriate to extracellular nutrient availability. One such example has been elucidated in yeast responding to nitrogen starvation, where increased trafficking to the vacuole is achieved through the amino acid sensing TORC1 complex, which activates Rsp5 adaptors via the Npr1 kinase and promotes cargo ubiquitination and degradation (MacGurn *et al.*, 2011). The Rag GTPases integrate with nutrient sensing and TORC1 activity via the EGO complex (Binda *et al.*, 2009; Bonfils *et al.*, 2012; Péli-Gulli *et al.*, 2015), but in addition regulate recycling via endosomally localized Ltv1 in response to extracellular leucine (MacDonald and Piper, 2017). Glucose starvation may also trigger a similar dual regulation of recycling and degradation pathways in yeast, where many metabolic pathways are evolutionarily conserved (Santangelo, 2006). Although most transcriptional changes elucidated in response to suboptimal glucose availability involve alternative carbon pathways, we recently revealed a response that increases trafficking from the surface to the lysosome in response to glucose starvation (Laidlaw *et al.*, 2020). Furthermore, recycling back to the surface is reduced when cells are exposed to media lacking sugar (Lang *et al.*, 2014), but the molecular players involved in this response are not fully established.

At high glucose levels, Snf1 (yeast AMP-activated protein kinase, AMPK [Hong *et al.*, 2003]) is inactivated primarily through its dephosphorylation by Reg1-Glc7 (Tu and Carlson, 1994; Sanz *et al.*, 2000). While Snf1 can influence endosomal trafficking during glucose changes in yeast independently (O'Donnell *et al.*, 2015), one key downstream consequence of glucose starvation involves Snf1 activation and regulation of the Mig1 transcriptional repressor (Johnston *et al.*, 1994; Treitel *et al.*, 1998). Mig1 is a zinc finger transcription factor that mediates glucose repression in yeast cells (Nehlin and Ronne, 1990; Lundin *et al.*, 1994) and in response activates alternative metabolic pathways (Schüller, 2003). In addition to this, Mig1 influences membrane trafficking machinery through its repression of clathrin adaptor genes *YAP1801* and *YAP1802* under glucose-replete conditions that stabilize endocytosis levels (Laidlaw *et al.*, 2020). Furthermore, the reduced recycling following glucose starvation (Lang *et al.*, 2014) can be bypassed by enforcing cargo ubiquitination in the endomembrane system upstream of MVB sorting (Buelto *et al.*, 2020). This suggests that both the ubiquitin-mediated degradation pathway (MacDonald and Piper, 2016) and the counteracting recycling pathway induced following cargo deubiquitination (MacDonald *et al.*, 2012a, 2015a) are both regulated in response to glucose starvation to collectively reduce surface activity and increased vacuolar degradation.

A genetic screen for recycling machinery identified several candidates for glucose-mediated control, including the G-protein–coupled receptor (GPCR) Gpr1 and downstream GTPase Ras2 (MacDonald and Piper, 2017). The Gα subunit Gpa2, which is activated Gpr1, initiates cAMP signaling in response to glucose through recruiting Ras-GTP to the PM (Colombo *et al.*, 1998; Broggi *et al.*, 2013). This cAMP signaling cascade in response to glucose leads to changes in a variety of different targets through protein kinase A (PKA) (Thevelein, 1994; Kraakman *et al.*, 1999). The screen for recycling machinery also implicated a distinct Gα subunit, Gpa1, in recycling (MacDonald and Piper, 2017). Gpa1 is the Gα subunit of a heterotrimeric G-protein complex also made up of Gβ and Gγ subunits Ste4p and Ste18p that functions in the pheromone response pathway (Dietzel and Kurjan, 1987; Miyajima *et al.*, 1987; Whiteway *et al.*, 1989). Just as Gpa2 cannot functionally couple with distinct mating GPCRs (Blumer and Thorner, 1990), it is thought that the distinct Gα subunit Gpa1 does not regulate Gpr1 directly. In addition to playing a role in pheromone response at the PM, Gpa1 interacts with the yeast phosphatidylinositol 3-kinase (Vps15 and Vps34) at endosomes (Slessareva *et al.*, 2006; Heenan *et al.*, 2009). The phosphorylation status of a variety of different phosphoinositide (PI) species regulates membrane trafficking pathways (Camilli *et al.*, 1996). Phosphoinositide 3-kinases (PI3Ks) are therefore key regulatory proteins known to control a variety of different membrane trafficking steps (Lindmo and Stenmark, 2006). Vps34, in complex with Vps15, was first identified in yeast as being required for the post-Golgi trafficking of biosynthetic enzymes to the vacuole (Herman and Emr, 1990; Schu *et al.*, 1993; Stack *et al.*, 1993), and generation of phosphatidylinositol 3-phosphates (PtdIns3P) through Vps34 activity is required for efficient retrograde recycling from the endosome to the late-Golgi (Burda *et al.*, 2002).

In this study, we use both lipid and protein recycling reporters to show that glucose starvation inhibits endosomal recycling of cargo back to the surface. We show that the Gα subunit Gpa1 and PI3K, and their functional association, are required for efficient recycling in glucose-replete conditions. During glucose starvation, we document Mig1-dependent elevation of Gpa2, which concentrates at the PM where it physically interacts with Gpa1. Increased levels of Gpa2 observed in glucose-starved cells impair production of PtdIns3P and result in recycling defects of a wide range of cargoes. We propose a role for Gpa2 as a glucose-responsive recycling inhibitor, potentially by commandeering Gpa1 from endosomal PI3K and ultimately serving to increase endosomal retention and vacuolar degradation of surface cargoes, as a survival response to glucose starvation.

RESULTS

Glucose starvation inhibits surface recycling

Previous work has shown that in response to glucose starvation, the yeast AP180 clathrin adaptors are transcriptionally up-regulated with a concomitant increase in endocytosis (Laidlaw *et al.*, 2020). Under basal conditions in media lacking methionine, the methionine transporter Mup1 tagged with GFP localizes to the PM, but much of this signal is redistributed to endosomes and the vacuole upon plasmid overexpression of mCherry-tagged AP180s: Yap1801-Cherry or Yap1802-mCherry (Figure 1A). In contrast, a recycling reporter based on the fusion of the GPCR Ste3 tagged with GFP and
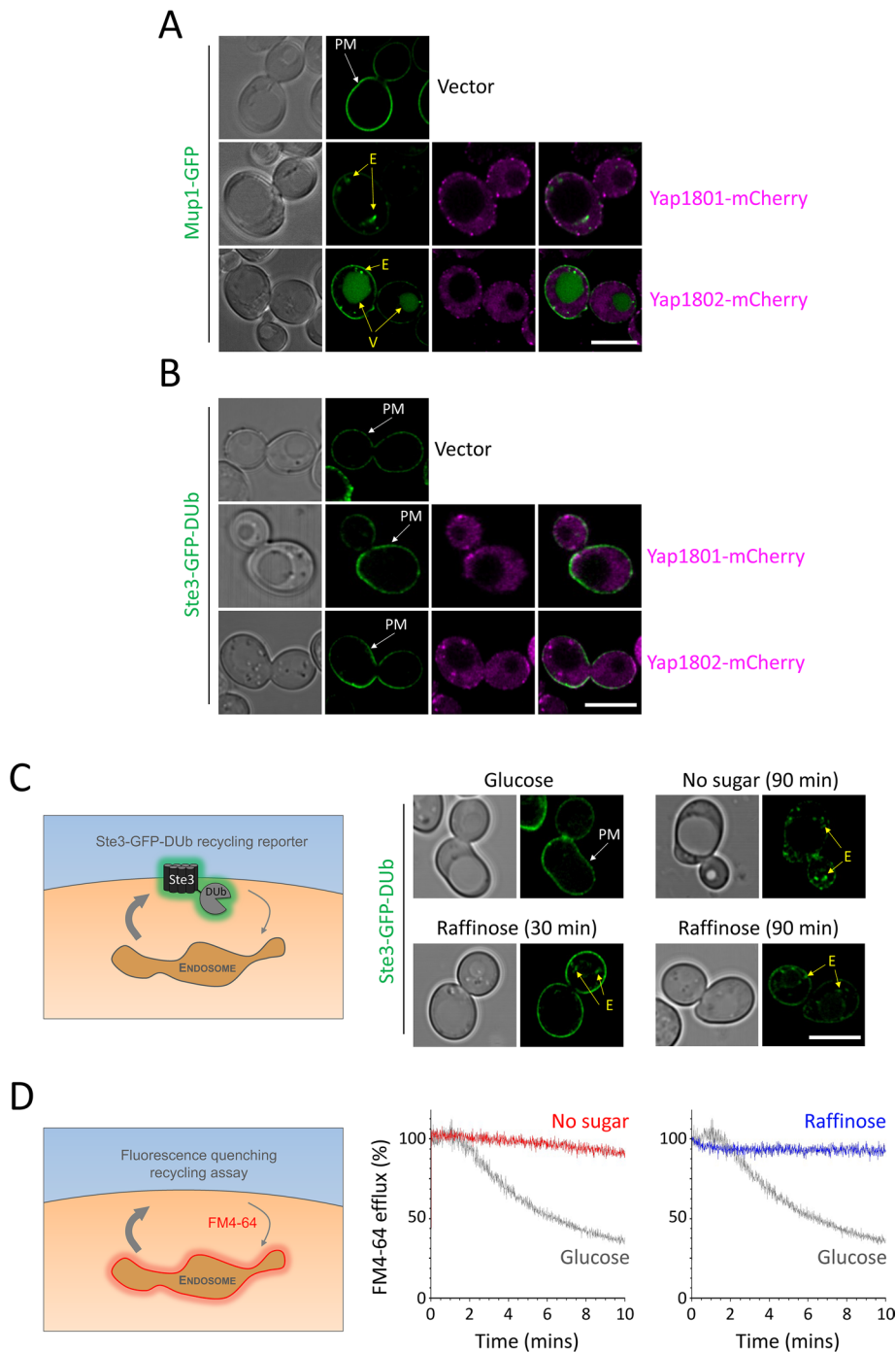
FIGURE 1: Glucose starvation specifically inhibits recycling. (A) Confocal imaging of cells expressing Mup1-GFP under control of its endogenous promoter coexpressed with Yap1801-mCherry or Yap1802-mCherry expressed from the *CUP1* promoter through addition of 50 μM copper chloride for 2 h. A vector control exposed to copper was also included. (B) Cells stably integrated with Ste3-GFP-DUb were exposed to 2 h copper chloride to induce expression of mCherry-tagged versions of Yap1801 and Yap1802 before confocal microscopy. (C) Cells expressing Ste3-GFP-DUb from the *STE3* promoter were grown under the indicated media conditions before confocal microscopy. (D) Wild-type cells were loaded with rich media containing 40 μM FM4-64 for 8 min before washing and dye efflux measured over time by flow cytometry. Control cells grown in glucose media were compared with 30-min prior incubation with media lacking any carbon source (red) or media supplemented with raffinose (blue). White arrows indicate exclusive PM signal, and yellow arrows indicate endosome (E) or vacuole (V) localizations. Scale bar, 5 μm.

the catalytic domain of a deubiquitinating enzyme (Stringer and Piper, 2011; MacDonald and Piper, 2017) showed no increase in endosomal localization following overexpression of yeast AP180s (Figure 1B). This correlates with observations that Ste3-GFP-DUb does not accumulate when endocytosis rates are elevated by the addition of a-factor or at elevated temperature (MacDonald and Piper, 2017). We conclude that although different manipulations increase the rate of endocytosis, the deubiquitination-driven recycling of Ste3-GFP-DUb predominates to maintain an exclusive steady state localization at the PM. Having established that Ste3-GFP-DUb primarily reports on cell surface recycling, we used this reporter to test whether glucose starvation impacts recycling specifically. Treating the cells in media completely lacking sugar, or by substituting glucose for the alternative carbon course raffinose, results in an accumulation of Ste3-GFP-DUb in intracellular endosomes (Figure 1C). A distinct recycling assay, which measures recycling by efflux of endocytosed fluorescent FM4-64 (Wiederkehr *et al.*, 2000), has previously shown that carbon source removal inhibits recycling (Lang *et al.*, 2014). Similarly, we find that shifting cells to media lacking sugar or supplemented with raffinose also results in robust inhibition of recycling (Figure 1D). Therefore, although internalization from the PM increases following glucose starvation (Laidlaw *et al.*, 2020), two dedicated recycling reporters show that glucose starvation also triggers a reduction in protein and lipid traffic from endosomes back to the PM. We propose that increased internalization and decreased recycling during glucose starvation cooperate to drive vacuolar degradation of cargoes en masse in response to nutritional stress. We set out to explain this recycling response at a molecular level. As both glucose removal and raffinose exhibit defects in recycling, we use raffinose substitution to deprive cells of glucose in downstream experiments, as it cannot be readily metabolized (de la Fuente and Sols, 1962) and therefore in the time frame we perform experiments provides a glucose starvation condition.

Gpa1-PI3K is required for surface recycling

A previous genetic screen for novel recycling machinery, based on the mislocalization of Ste3-GFP-DUb (MacDonald and Piper, 2017), identified 89 candidate factors as required for recycling (Figure 2A). To
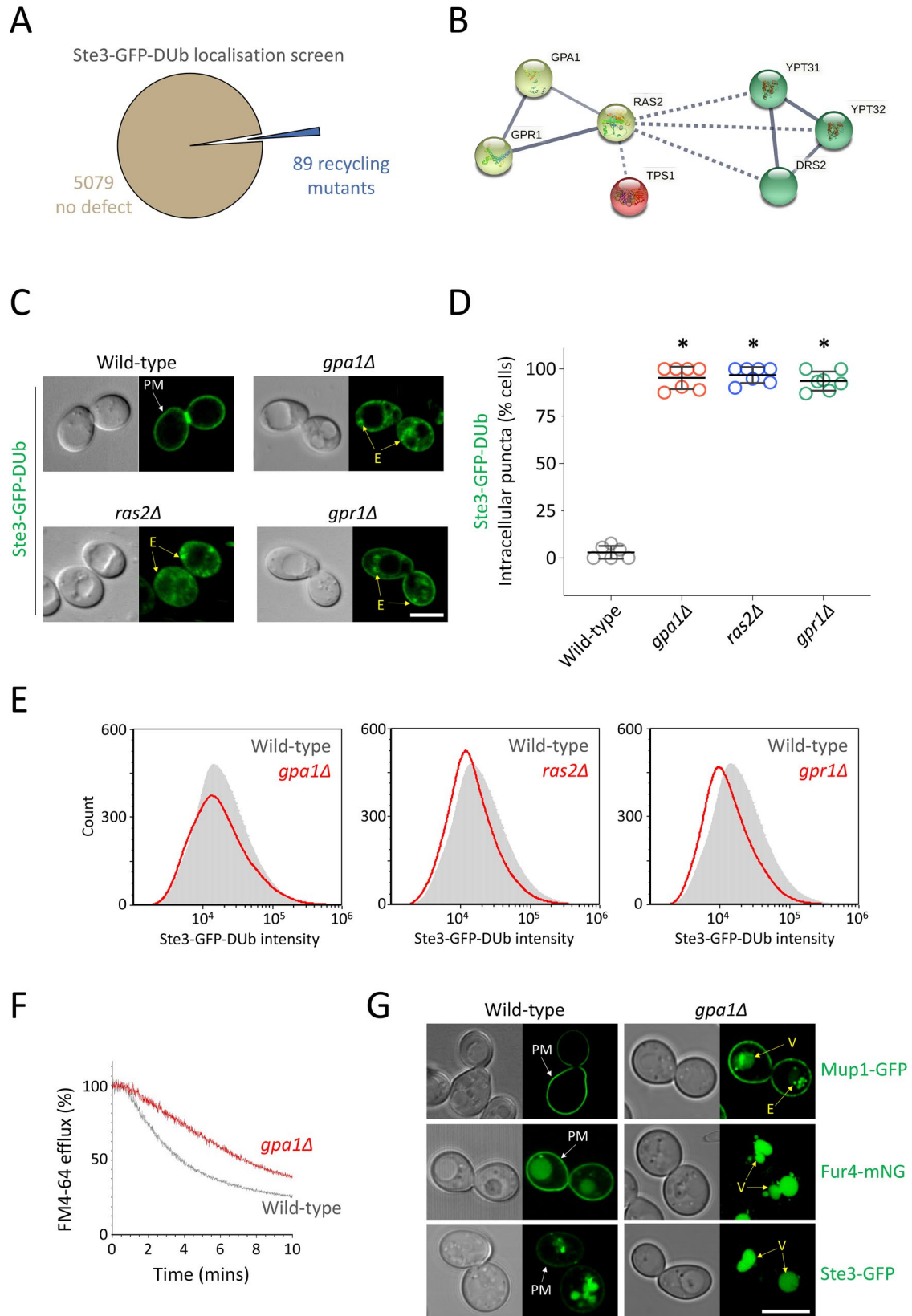
FIGURE 2: Gpa1 is required for protein and lipid recycling to the surface. (A) Pie chart representing gene deletions that have no impact on Ste3-GFP-DUb recycling (brown) or those that accumulate the reporter in endosomes (blue). (B) String pathway analysis was performed on all 89 recycling factor candidates (minimum interaction score = high confidence, 0.700) before application of a *k*-means clustering algorithm to define nine groups. A small cluster connected by solid lines, representing strongly supported functional and physical associations (yellow), is shown alongside associations with distinct clusters (red and green) shown by broken lines. (C) Ste3-GFP-DUb localization recorded in the

identify any proteins from this list that might inhibit recycling during glucose starvation (Figure 1), a network analysis of all 89 proteins was performed based on both physical and functional associations to reveal a small cluster, containing the glucose-regulated receptor Gpr1 and associated factors Ras2 and Gpa1 (Figure 2B). We stably integrated the Ste3-GFP-DUb reporter into strains lacking each factor (*gpa1Δ*, *ras2Δ*, and *gpr1Δ*) and confirmed that they exhibit defects in recycling (Figure 2, C and D). Although deletion of these genes results in a pronounced mislocalization phenotype, we also performed flow cytometry experiments to confirm that total levels of Ste3-GFP-DUb were not elevated to account for additional signal in intracellular compartments (Figure 2E). Although all three candidates are known to localize and function at the PM, we focused on the Gα subunit Gpa1 for this study, as it has also been shown to localize to endosomes and activate PI3K (Slessareva *et al.*, 2006), which is involved in various endomembrane trafficking events (Lindmo and Stenmark, 2006; Reidick *et al.*, 2017). We first considered that the G-protein subunit Gpa1 might specifically perturb the Ste-GFP-DUb reporter, as it is based on the G-protein–coupled receptor Ste3. However, we found that general recycling of lipids, as assessed by FM4-64 efflux, was also defective in *gpa1Δ* mutants (Figure 2F). Furthermore, trafficking of endogenous cargoes to the PM was also perturbed in *gpa1Δ* cells. We found that the methionine transporter Mup1 tagged with GFP, which localizes exclusively to the PM in wild-type cells, is shifted to endosomes and the vacuole in *gpa1Δ* mutants (Figure 2G). Similarly, the PM signal of the uracil transporter Fur4, tagged with mNeonGreen (mNG) (Paine *et al.*, 2021), or Ste3, tagged with GFP (but lacking a deubiquitinating enzyme fusion), was sorted to the vacuole in *gpa1Δ* cells. These defects in lipid and protein trafficking are consistent with a role for Gpa1 in surface recycling.

Constitutive signaling in haploid *gpa1Δ* mutants is lethal (Miyajima *et al.*, 1987), so we first confirmed *GPA1* deletion in both our Mata and Matα backgrounds by genotyping (Figure 3A) and genome sequencing (Figure 3B). We surveyed all genetic mutations identified from both *gpa1Δ* mutants and wild-type cells and found that most variants were distanced from open reading frames (ORFs), so unlikely to affect expression, or missense variants unlikely to alter function. Gene ontology of mutated genes revealed a premature stop codon in the *STE11* gene of Mata *gpa1Δ* cells (Figure 3, C and D), which would perturb downstream signaling and suppress lethality (Nakayama *et al.*, 1988). An explanation of suppression in Matα mutants is less clear but it might be due to a substitution in the downstream mitogen-activated protein (MAP) kinase kinase (MAPKK) *MKK1*. This alone, or in combination with a parental strain point mutation in *SST2*, which encodes a negative regulator of Gpa1 signaling (Dohlman *et al.*, 1996; Apanovitch *et al.*, 1998), might explain viability of *gpa1Δ* mutants.

To test whether these Gpa1 effects are mediated through PI3K, we analyzed recycling in cells lacking PI3K subunits (*vps15Δ* and *vps34Δ*), both of which exhibit morphological defects of the vacuolar/endolysosomal system (Figure 4A). Vacuole morphology following FM4-64 staining was difficult to resolve by conventional confocal

microscopy but Airyscan microscopy revealed layers of small vacuolar-like structures in both *vps15Δ* and *vps34Δ* cells. Both *vps15Δ* and *vps34Δ* mutants were confirmed to have a growth defect at 30°C (Figure 4B) before we revealed that *vps15Δ* and *vps34Δ* cells are severely defective in their ability to recycle internalized FM4-64 dye (Figure 4C). To further corroborate this model, we employed a hyperactive version of Vps34, termed Vps34^{EDC} (harboring R283E, A287D, and Y501C point mutations), that was recently used to show that PtdIns3P production is rate limiting for some, but not all, membrane trafficking pathways (Steinfeld *et al.*, 2021). We found that unlike deletion of PI3K, increased expression of Vps34^{WT} or Vps34^{EDC} had no effect on growth at 30°C (Figure 4B). However, expressing hyperactive Vps34^{EDC} was sufficient to perturb efficient recycling of FM4-64 (Figure 4D) and Ste3-GFP-DUb (Figure 4E), suggesting that elevated PtdIns3P production deregulates recycling, but to a lesser degree than in cells lacking PI3K activity. To test whether a functional connection between Gpa1 and PI3K is required for efficient recycling, we created an R1261A mutation in endogenous Vps15 (Figure 4, F and G) that disrupts interaction with Gpa1 (Heenan *et al.*, 2009) and found that this was sufficient to inhibit efficient FM4-64 recycling (Figure 4H). This supports the notion that yeast PI3K in collaboration with Gpa1 is responsible for recycling from endosomes to the surface.

Reg1 regulates recycling at transcriptional level

Gpa1 localizes to the PM and endomembrane compartments (Slessareva *et al.*, 2006; Dixit *et al.*, 2014). Fluorescently tagged Gpa1, which functionally complements *gpa1Δ* cells (Supplemental Figure S1), colocalizes with the late endosome marker Vps4, and to a lesser degree, the TGN marker Sec7 (Figure 5A). We found that there was a subtle defect in Ste3-GFP-DUb recycling upon overexpression of Gpa1-mCherry (Figure 5B), suggesting that both PI3K and Gpa1 levels need to be finely tuned for efficient recycling back to the surface. Intracellular Ste3-GFP-DUb colocalized with Gpa1-mCherry in both wild type and recycling defective *rcy1Δ* mutants, suggesting a trafficking block in endosomes from which recycling occurs. Expressing a constitutively active version (Gpa1^{Q323L}-mCherry) caused more severe defects in Ste3-GFP-DUb recycling (Figure 5, C and F), again with endosomal reporter colocalizing with Gpa1. Intriguingly, the Gpa1^{Q323L} screen that revealed Gpa1 couples with PI3K during PtdIns3P production (Slessareva *et al.*, 2006) also demonstrated that the glucose-related phosphatase *REG1* is functionally associated Gpa1 (Figure 5D). To explore whether the recycling defects associated with Gpa1-PI3K are related to glucose-mediated recycling, we tested recycling in *reg1Δ* mutants and found that both Ste3-GFP-DUb (Figure 5, E and F) and FM4-64 (Figure 5G) do not efficiently recycle. No obvious recycling defects were observed in cells lacking the distinct *SNF3* glucose-sensing component. We hypothesized that the connection between glucose/Reg1 and Gpa1/PI3K allowed cargo recycling from endosomes to the surface to be regulated in response to available glucose.

Reg1, alongside the essential phosphatase Glc7 and the yeast AMPK family member Snf1, participates in a signal transduction

---

indicated cells by confocal microscopy. (D) Quantification of Ste3-GFP-DUb intracellular localizations calculated as an average of population (*n* = 3) from wild type = 90; *gpa1Δ* = 75; *ras2Δ* = 94; and *gpr1Δ* = 70 cells. (E) Flow cytometry was used to measure Ste3-GFP-DUb fluorescence from approximately 75,000 cells of each indicated mutant (red) and compared with expression in wild-type cells (gray overlay). (F) Wild-type (gray) or *gpa1Δ* (red) cells were loaded with FM4-64 for 8 min before dye efflux was assessed by flow cytometry over 10 min. (G) Wild-type and *gpa1Δ* cells expressing Mup1-GFP, Fur4-mNG, or Ste3-GFP were grown to log phase before confocal microscopy to determine localization. White arrows (exclusive PM) and yellow arrows (vacuole; V) are indicated. Scale bar, 5 μm.
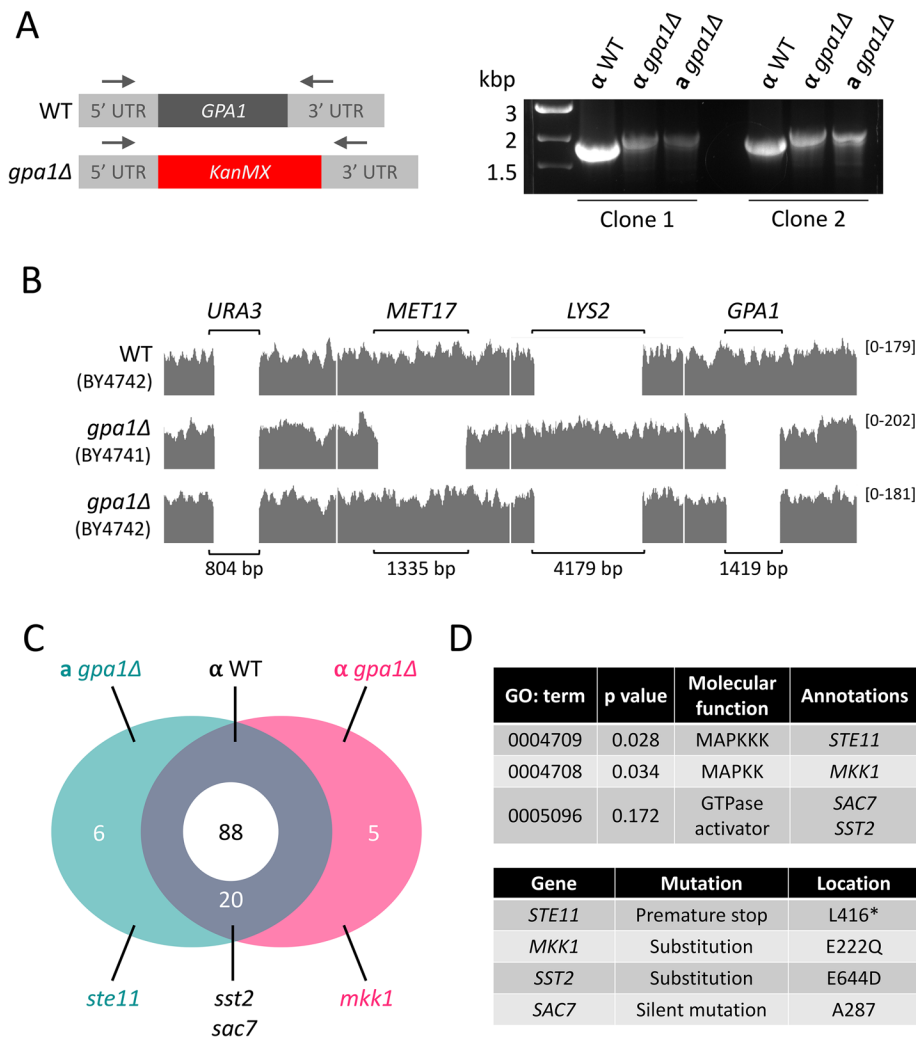
FIGURE 3: Genetic validation of viable *gpa1Δ* mutant yeast strains. (A) Schematic depicting region of the genome that was PCR amplified using oligos in 5′ and 3′ UTRs of *GPA1* (left). genomic DNA was isolated from Matα (wild-type and *gpa1Δ*) and Mata *gpa1Δ* cells and used for PCR confirmation of the *KanMX* deletion cassette in *gpa1Δ* mutants (right). (B) Genome sequencing was performed on cells described in A with read-depth visualized in Integrative Genomics Viewer (IGV) software for the specific loci shown: *URA3*, deleted in both BY-parental strains; *MET17* deleted in BY4741; *LYS2* deleted in BY4742; and *GPA1*, deleted in *gpa1Δ* cells in both mating types. (C) Venn diagram depicting the overlapping gene mutations related to Gpa1 found in sequenced strains. (D) List of enriched annotations from gene ontology (GO) analysis related to mating and Gpa1 signaling (top) and specific mutation details of identified mutations (bottom).

cose starvation or in either *reg1Δ* or *gpa1Δ* cells. As a glucose-responsive inhibitor, transcript levels of *GPA2* would increase Gpa2 protein levels following glucose starvation, which would consequently inhibit Gpa1 recycling (Figure 6B). This model would predict that elevated levels of PM localized Gpa2 interacting with Gpa1 would hamper the finely tuned production of PtdIns3P via Gpa1-PI3K required for efficient surface recycling.

Gpa2 inhibits surface recycling

We find that recycling defects of *gpa1Δ* cells are phenocopied in *reg1Δ* mutants (Figures 2, C and E, and 5, E and F). We reasoned that if the functional role of Reg1 in recycling is through its capacity to modulate transcription via the Reg1/Glc7 > Snf1 > Mig1/2 pathway, then recycling defects of *reg1Δ* cells would also be phenocopied in *mig1Δ mig2Δ* mutant cells. Alternatively, if recycling is efficient in *mig1Δ mig2Δ* cells, a direct role between Reg1 and its substrate Gpa1 (Clement *et al.*, 2013) might best explain the data. Mig1 is a glucose-sensitive transcriptional repressor that rapidly translocates from the nucleus when cells are shifted to raffinose media (Figure 7, A and B, and Supplemental Figure S2). Many glucose-repressed genes are transcriptionally up-regulated upon glucose starvation or in *mig1Δ mig2Δ* cells lacking the repressors (Westholm *et al.*, 2008). As *mig1Δ mig2Δ* mutants exhibit perturbed Ste3-GFP-DUb recycling (Figure 7C), we assume that recycling defects in *reg1Δ* mutants are explained via a transcriptional response, as discussed (Figure 6). To identify genes transcriptionally controlled by Reg1>Mig1 that inhibit Gpa1-mediated recycling, we cross-referenced a list of genes predicted to be repressed by Mig1 (Wollman *et al.*, 2017) with the physical interactome of Gpa1 to reveal only one candidate, Gpa2 (Figure 7D). To test whether *GPA2* was a bona fide target gene for Mig1 repression controlled by glucose, we performed quantitative RT-PCR experiments. First, we revealed that *GPA1* transcript levels are unchanged in response to Mig1 repression or available glucose. In contrast, the proposed Gpa1-inhibitor *GPA2* is transcriptionally up-regulated ~2.0 ± 0.3-fold in *mig1Δ mig2Δ* cells and ~6.4 ± 0.7-fold upon a shift to raffinose for 1 h (Figure 7E). This transcriptional profile is consistent with overexpression of a Gpa1 recycling inhibitor. Similarly, deletion of the proposed inhibitor exhibits no defects in Ste3-GFP-DUb recycling (Figure 7F), suggesting that only increasing levels of Gpa2 inhibit recycling. We did find that *gpa1Δ gpa2Δ* cells are defective for Ste3-GFP-DUb recycling, supporting the idea that while Gpa1-PI3K is required for recycling, Gpa2 is a downstream regulator. The Ste3-GFP-DUb recycling defects triggered by deletion of *MIG1* and *MIG2* can be attributed to the induced levels of Gpa2 in these

pathway that controls transcription in response to glucose (Tu and Carlson, 1994, 1995; Ludin *et al.*, 1998; Sanz *et al.*, 2000). Snf1 regulates the Mig1 transcriptional repressor in response to glucose levels to repress various metabolic genes (Johnston *et al.*, 1994; Vallier and Carlson, 1994; Treitel *et al.*, 1998). We considered a model whereby this signaling mechanism maintained high levels of surface cargoes in glucose-replete conditions by repression of a recycling inhibitor that acts on Gpa1-PI3K (Figure 6A). We went on to identify one candidate inhibitor (discussed below), the Gα subunit Gpa2, which physically and genetically interacts with Gpa1 (Xue *et al.*, 1998; Ho *et al.*, 2002), that we propose fulfills the function of Gpa1-recycling inhibitor. This model would predict that deletion of *MIG1* and *MIG2* repressors (Lutfiyya *et al.*, 1998; Westholm *et al.*, 2008) would phenocopy the defective recycling observed followed by glu-

FIGURE 4: Defined PI3-kinase activity is required for efficient surface recycling. (A) Confocal and Airyscan imaging of wild-type, *vps15Δ*, and *vps34Δ* cells first labeled with 10 µM FM4-64 for 30 min, followed by washing and a 1-h chase in SC minimal media. (B) The indicated cells were grown to log phase, equivalent volumes harvested, and a 1 in 10 serial dilution spotted onto YPD and SC media and incubated at 30°C. (C, D) The indicated strains and transformants were loaded with 40 µM FM4-64 in rich media for 8 min before three 5 min washes, and FM4-64 dye efflux measured over time by flow cytometry and plotted by the % of the initial 10 s fluorescence. (E) Wild-type cells coexpressing Ste3-GFP-DUb with either Vps34^WT or Vps34^EDC were imaged using confocal microscopy. (F) Surface model of Vps15 WD-repeat domain (gray) with R1261 shown (magenta). (G) Sequencing results of the *vps15^R1261A* allele confirmed by Sanger sequencing of PCR product generated from genomic DNA. (H) FM4-64 efflux was assessed following the protocol in C for the indicated strains. Scale bar, 5 µm.

Gpa1-mCherry partially colocalizes, in addition to its endosomal localization. However, this endosomal population shifts to primarily PM in *rcy1Δ* recycling mutants (Supplemental Figure S3).

We next confirmed that this Mig1-based transcriptional response results in an increase in Gpa2-GFP protein levels by immunoblot following 2-h raffinose treatment (Figure 8, A and B). By assessing maximum-intensity projects from three-dimensional (3D) Airyscan imaging of cells expressing Gpa2-GFP, we also found a pool of cytosolic Gpa2-GFP in glucose-grown cells that redistributes to the PM following raffinose treatment (Figure 8, C and D). Similar analysis of 3D images focusing only on the top or bottom of cells also revealed punctate PM accumulations of Gpa2-GFP in raffinose-grown cells (Figure 8, E and F), but it is unclear whether these have functional significance or are indirectly due to the influx of higher protein levels and greater surface/cytoplasm ratios. Our model predicts that elevated levels of Gpa2 would inhibit recycling, which was confirmed by overexpressing plasmid-borne fluorescently tagged versions of Gpa2, which we confirmed are functional (Supplemental Figure S4). We find that overexpressed Gpa2-mCherry triggered accumulation of Ste3-GFP-DUb in intracellular compartments (Figure 9, A and B). Similarly, cells overexpressing Gpa2-GFP have reduced efflux of FM4-64 from the recycling pathway, when compared with control cells expressing the methionine transporter Mup1-GFP (Figure 9C and Supplemental Figure S5). In addition to these recycling-specific cargoes, we also used the Gpa2-mCherry overexpression system to reveal prominent defects in recycling of the PM-localized GFP-tagged transporters Mup1 and Can1, which shift to endosomes and the vacuole (Figure 9D). Gpa2 overexpression induced a reduction of Ste3-GFP from the PM; however, we also note that vacuolar sorting, which is typically evident in wild-type cells at steady state, is blocked following Gpa2-mCherry overexpression, and cargo accumulates in prevacuolar structures. We assume overexpression of the Gα subunit Gpa2 perturbs trafficking of Ste3 in a manner distinct from general Gpa1-PI3K lipid-mediated trafficking. As Ste3 is a GPCR, excess Gpa2 might force it to adopt a conformation at the PM that is not conducive to MVB sorting.

To explore whether Gpa2 could function at endosomes directly, we performed time-lapse microscopy of cells expressing Gpa2-GFP and only very rarely observed intracellular puncta; however, these did not colocalize with Gpa1-mCherry (Figure 10A). We did find strong accumulations

cells, as additionally deleting *GPA2* in a *mig1Δ mig2Δ* background suppresses recycling defects (Figure 7G). We found that cells expressing Gpa2-GFP localized almost exclusively to the PM, where
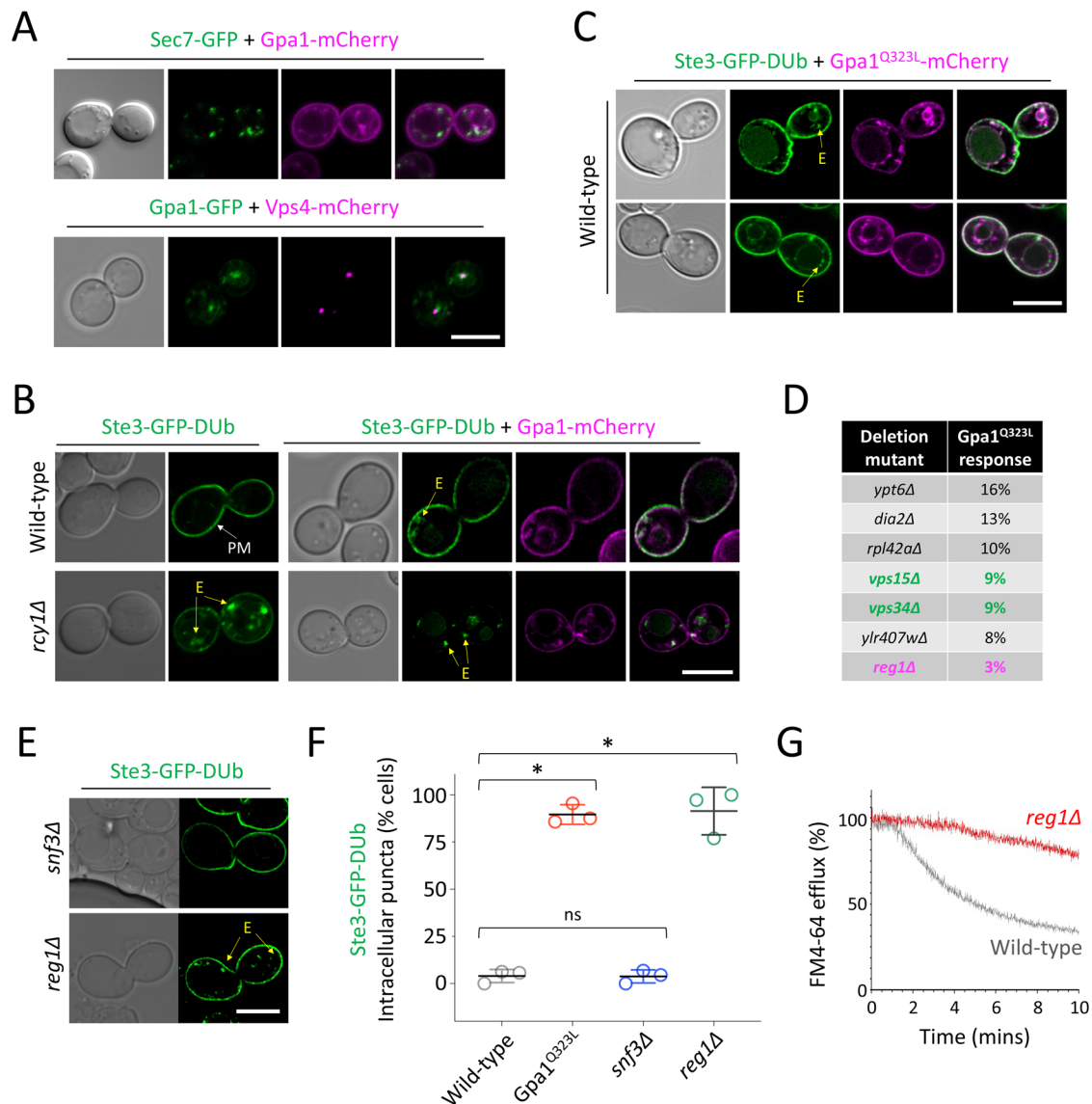
FIGURE 5: Reg1 is a proposed upstream Gpa1 regulator in recycling. (A) Confocal microscopy of wild-type cells co expressing Sec7-GFP and Gpa1-mCherry (top) and Gpa1-GFP and Vps4-mCherry (bottom). (B) Wild-type and *rcy1Δ* cells expressing Ste3-GFP-DUb with and without Gpa1-mCherry were imaged by confocal microscopy. (C) Ste3-GFP-DUb localization in wild-type cells coexpressing Gpa1^{Q323L}-mCherry was assessed by fluorescence microscopy. (D) Top-scoring mutants from a Gpa1^{Q323L} mating response screen (Slessareva *et al.*, 2006) are shown, with PI3K mutants (green) and *reg1Δ* (magenta) highlighted. (E) Confocal microscopy of *snf3Δ* and *reg1Δ* cells stably expressing Ste3-GFP-DUb. (F) Quantification of Ste3-GFP-DUb intracellular localizations calculated as an average of population (n = 3) from WT = 68; Gpa1^{Q323L} = 51; *snf3Δ* = 83; and *reg1Δ* = 73 cells. (G) Wild-type (gray) and *reg1Δ* (red) cells were incubated with rich media containing 40 μM FM4-64 for 8 min before washing and FM4-64 dye efflux measured over time by flow cytometry and plotted by the % of the initial 10 s fluorescence. Scale bar, 5 μm.

of Gpa2-GFP within subdomains of the PM, which are distinct from Mup1-GFP localization and partially colocalize with brief pulses of the endocytic dye FM4-64 (Figure 10B). To assess Gpa2-GFP localization across the entire cell, we optimized fast yet gentle Apotome structured illumination microscopy (SIM) imaging to capture fluorescence across the entire cell volume, with 42 distinct z-stack slices in both color channels, captured in only 4.3 s. Initial experiments were calibrated using the vacuolar cargo Cos5 (MacDonald *et al.*, 2015a). Cos5-GFP accumulates in the vacuole of wild-type cells but concentrates in class E endosomes in *vps25Δ* mutant cells (Supplemental Figure S6), so we used a dual-tagged Cos5-GFP-mCherry to optimize processing and noise correction (Figure 10C). 4D Apotome

SIM experiments show that Gpa2-GFP displays a continuous network distribution pattern across the PM (Figure 10D) reminiscent of the localization of the Gpa2-associated protein Ras2 (Spira *et al.*, 2012) but no colocalization with mCherry-tagged markers for the TGN and the MVB (Figure 10E and Supplemental Figure S7). As these efforts did not provide strong evidence for Gpa2 localizing anywhere other than the surface, we propose that the function of higher levels of Gpa2 at the PM during glucose starvation could simply be to appropriate more Gpa1, thereby depriving PI3K of Gpa1 and reducing its capacity to mediate efficient recycling. In support of this idea, we reveal a significant Förster resonance energy transfer (FRET) signal between Gpa2-GFP and Gpa1-mCherry
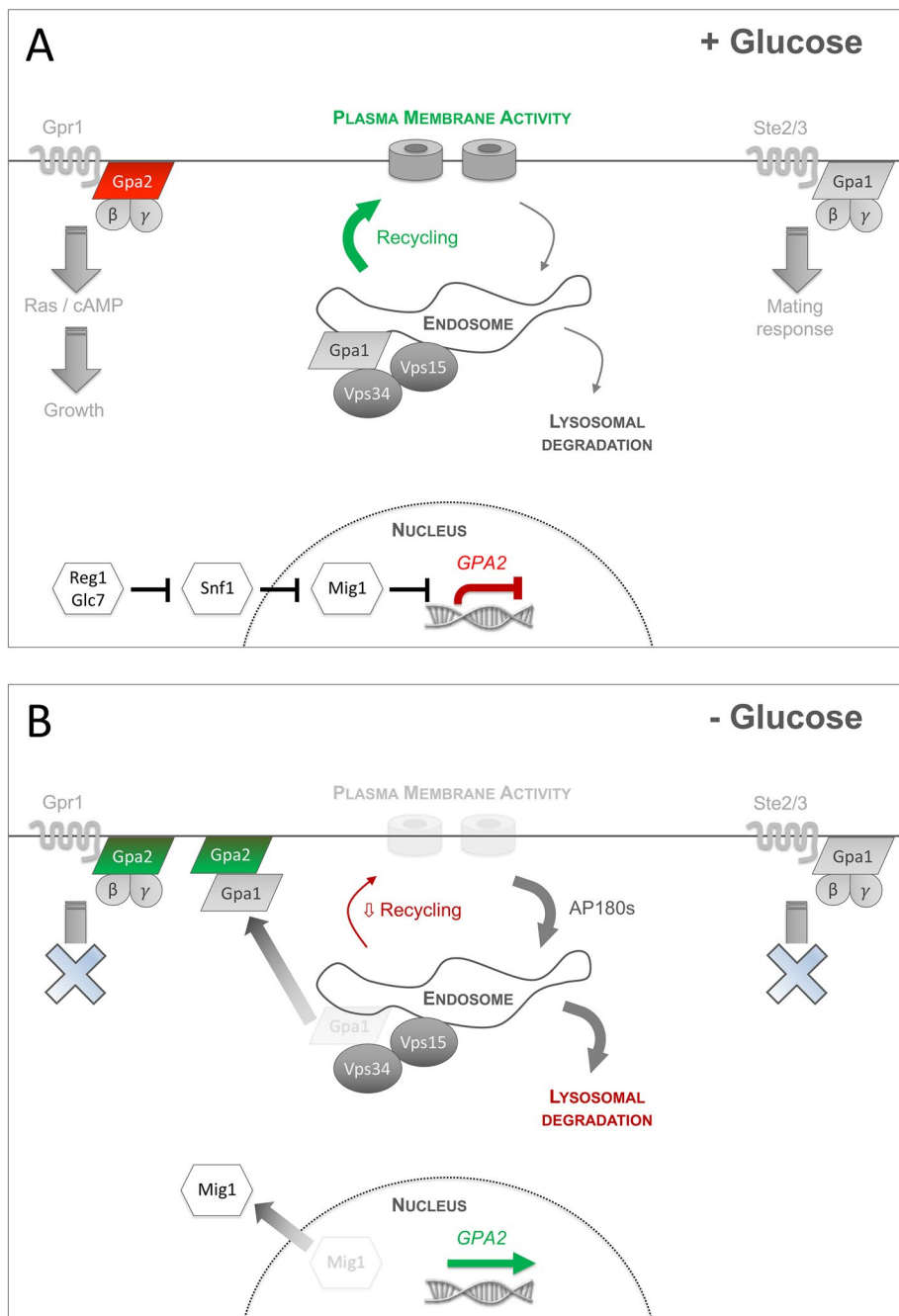
FIGURE 6: Model for glucose-mediated control of cargo recycling. (A) In glucose-rich conditions, metabolism of the cell is maintained to promote growth, in part through the cAMP synthesis pathway sensed through the GPCR Gpr1 and heterotrimeric G-protein alpha subunit, Gpa2. In glucose conditions, we propose that *GPA2* expression is suppressed via the established glucose repression pathway involving Glc7/Reg1 > Snf1 > Mig1. The pheromone signaling and mating pathway, controlled through haploid-specific GPCRs Ste2/Ste3, also functions at the PM via the G-protein alpha subunit, Gpa1. Gpa1 also has a function at endosomes, with PI3kinase subunits Vps15/Vps34 producing PtdIns3P. Surface recycling of PM cargoes is efficient in glucose-replete conditions, via an active and efficient recycling pathway from endosomes back to the surface. (B) Glucose starvation triggers several metabolic changes, including growth arrest sensed via Gpr1. This is accompanied by a reduction in mating response, as the Ste2/3 receptors are down-regulated. The Glc7 > Snf1 pathway results in dephosphorylation and translocation of nuclear repressor Mig1. In consequence, the yeast AP180 clathrin adaptors are transcriptionally up-regulated and induce higher levels of internalization from the PM. Concomitantly, levels of *GPA2* are increased, which we propose act as inhibitors of Gpa1-mediated recycling, potentially through sequestering more Gpa1 at the PM and therefore decamping from PI3K at the endosome and disrupting the lipid organization required to efficiently promote recycling.

at the surface (Figure 10, F and G, and Supplemental Figure S8), but no indication of FRET between Gpa1 and Sec7 or in unbleached controls. Finally, we show that PI3K production of PtdIns3P is impaired in raffinose-treated cells, indicated by the mislocalization of the PX-domain protein Snx41 and the FYVE-domain protein Pib1 (Figure 11, A and B), both of which bind endosomal membranes rich in PtdIns3P produced by PI3K (Burd and Emr, 1998; Shin *et al.*, 2001; Yu and Lemmon, 2001; Hettema *et al.*, 2003). These mislocalization effects were phenocopied in glucose-grown cells overexpressing Gpa2 from a plasmid.

DISCUSSION

Many protein and lipid trafficking itineraries are overhauled following acute nutrient depletion to equilibrate the energy balance of the cell and adjust metabolism appropriately for the change in extracellular conditions. Reduced recycling of material from endosomal compartments back to the PM benefits the cell by reducing anabolic load. Furthermore, surface proteins that are not recycled can be directed to the vacuolar degradation pathway instead and promote survival via catabolic processes. The division of labor between recycling and degradation pathways is not fully understood. Many surface proteins in yeast routinely accumulate in the vacuole, where fluorescent tags are stable, potentially overinflating the predominance of the well-characterized degradation pathway. Ubiquitination of surface cargoes is sufficient to mediate their sorting via the ESCRT-driven MVB pathway (Katzmann *et al.*, 2001; Urbanowski and Piper, 2001; Babst *et al.*, 2002a,b). Most vacuolar cargoes are ubiquitinated by the Rsp5 E3-ligase and its cargo-specific adaptors (O'Donnell and Schmidt, 2019; Sardana and Emr, 2021), but other ligases, such as Tul1 and Pib1, also contribute (Reggiori and Pelham, 2002; Li *et al.*, 2015; MacDonald *et al.*, 2017; Yang *et al.*, 2020). Employing a ubiquitination reversal strategy, achieved by fusion of cargo, E3-ligases, or ESCRT subunits to the catalytic domain of a deubiquitinating enzyme blocks cargo trafficking through the degradation pathway and allows focus on other endosomal trafficking events (Stringer and Piper, 2011; MacDonald *et al.*, 2012b, 2015b). Here, we show that the GPCR Ste3, tagged with GFP and a DUb domain (Ste3-GFP-DUb), recycling is specifically inhibited following glucose starvation, with Ste3-GFP-DUb accumulating in endosomes. We assume that efficient recycling of Ste3-GFP-DUb in wild-type cells maintains steady state signal at the PM, as increased internalization
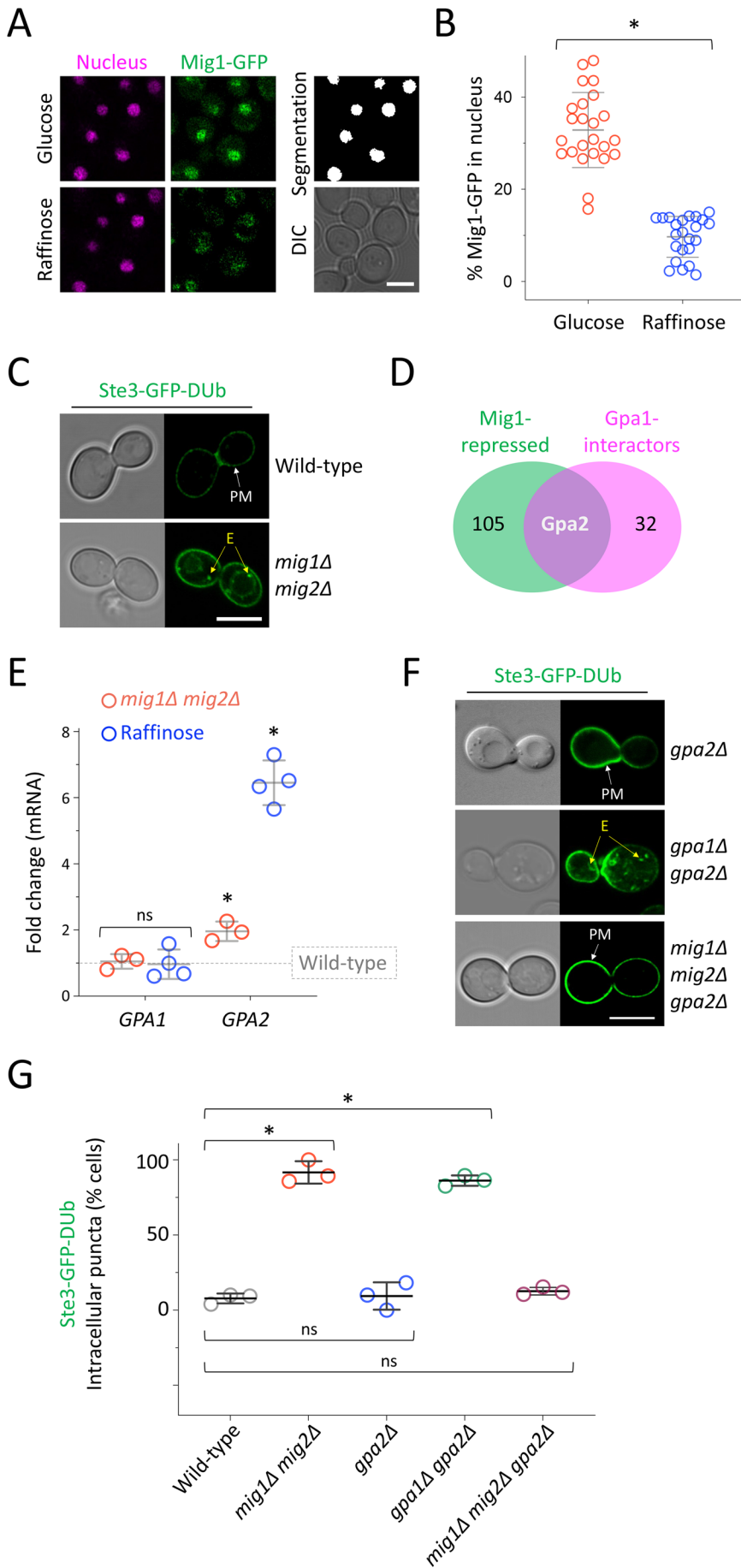
through overexpression of the yeast AP180 adaptors (Figure 1A) or pheromone or temperature is insufficient to accumulate Ste3-GFP-DUb in endosomes (MacDonald and Piper, 2017). Additionally, irrespective of the internalization rates of FM4-64 to endosomes (Vida and Emr, 1995), we find that glucose starvation inhibits FM4-64 recycling back to the PM, measured as a percentage of internalized dye that subsequently effluxes (Wiederkehr *et al.*, 2000). Therefore, we conclude that the Ste3-GFP-DUb reporter is a highly specific recycling reporter and that recycling of both protein and lipids is reduced in response to acute glucose starvation. A genetic screen for defects in Ste3-GFP-DUb recycling implicated the Gα subunit Gpa1 as required for recycling (MacDonald and Piper, 2017), which we confirmed by stably expressing Ste3-GFP-DUb in *gpa1Δ* cells to show that recycling is perturbed. Furthermore, *gpa1Δ* mutants cannot recycle FM4-64 as efficiently as wild-type cells and display either reduced PM signal or enhanced vacuolar sorting of various fluorescently tagged cargoes (Figure 2); the latter phenotype could be explained as an indirect consequence of reduced recycling.

Gpa1 has a role outside of surface GPCR signaling and can functionally connect with the yeast PI3K, composed of Vps34 and Vps15, to simulate PtdIns3P synthesis at endosomes (Slessareva *et al.*, 2006). Like *gpa1Δ* mutants, we

FIGURE 7: Glucose and Mig1-controlled expression of recycling inhibitor *GPA2*. (A) Confocal microscopy of wild-type cells coexpressing Mig1-GFP (green) and Nrd1-mCherry as a nuclear marker (magenta) under glucose-replete conditions. The same cells were imaged 5 min later following a raffinose exchange performed with microfluidics. (B) The percentage of nuclear Mig1-GFP signal under glucose and raffinose conditions was quantified (see *Materials and Methods*). * indicates unpaired Holm–Sidak t test ($p < 0.0001$). (C) Confocal microscopy of wild-type and *mig1Δmig2Δ* cells expressing Ste3-GFP-DUb. (D) Venn diagram of Mig1-repressed candidates (green) and proteins that physically interact with Gpa1 (magenta). (E) RT-qPCR was used to measure transcript levels of the indicated genes, compared with *ACT1*, in wild-type vs. *mig1Δ mig2Δ* (red) and wild-type cells grown in glucose vs. 60-min raffinose media (blue). Unpaired Holm–Sidak t tests showed that *GPA1* levels were not significantly (ns) altered in either experiment ($p = 0.748$ and 0.907, respectively) but levels of *GPA2* increased in both *mig1Δ mig2Δ* ($p < 0.001$) and raffinose ($p < 0.00001$). (F) Confocal microscopy of the indicated mutants expressing Ste3-GFP-DUb. (G) Quantification of Ste3-GFP-DUb intracellular localizations calculated as an average of population ($n = 3$) from WT = 77; *mig1Δ mig2Δ* = 64; *gpa2Δ* = 69; *gpa1Δ gpa2Δ* = 79; and *mig1Δ mig2Δ gpa2Δ* = 87 cells. Scale bar, 5 µm.
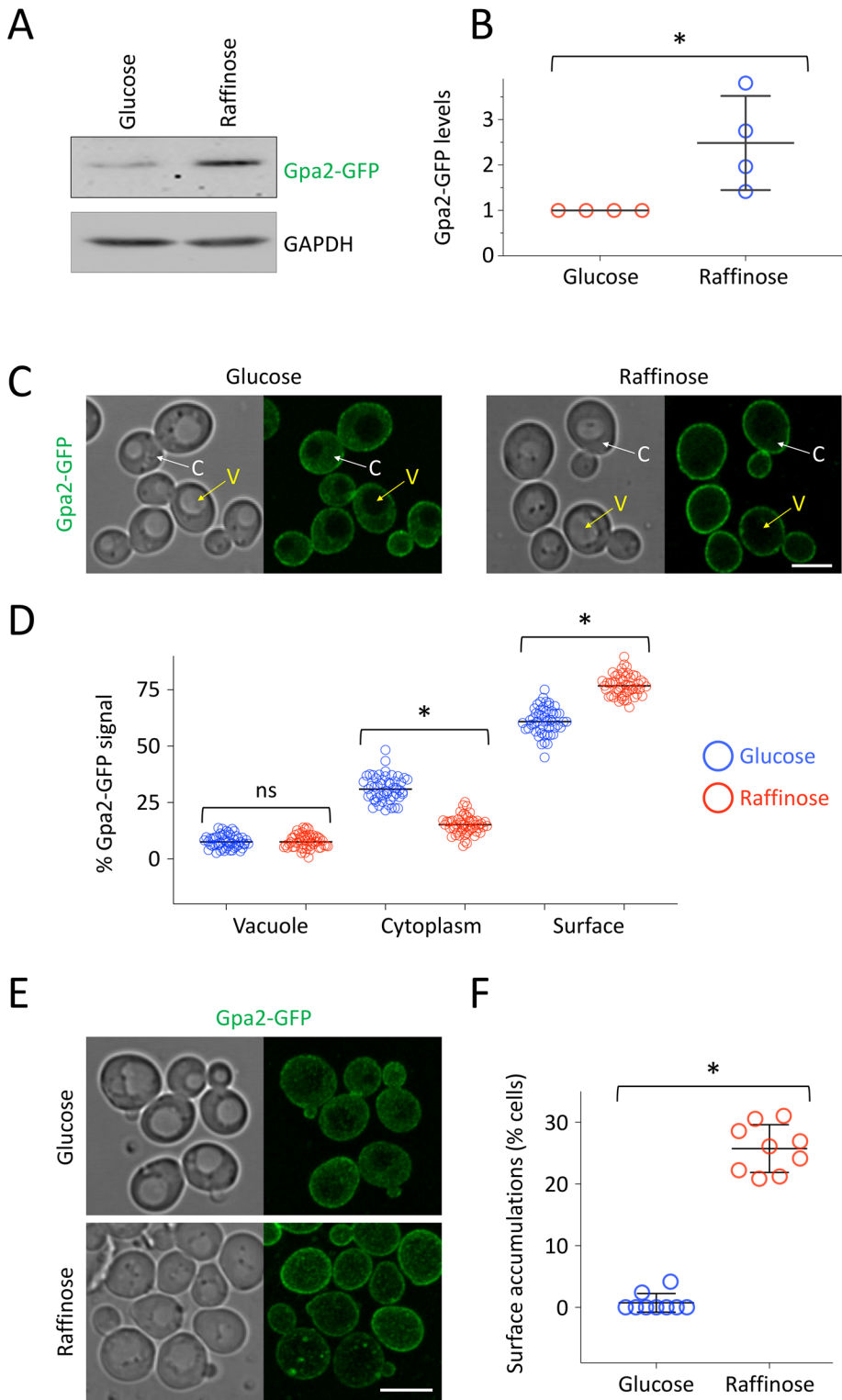
FIGURE 8: Glucose starvation–induced expression and surface concentration of Gpa2-GFP. (A) Wild-type cells expressing GFP-tagged Gpa2 were grown in glucose and 90 min raffinose conditions before lysates were made for immunoblot analysis probing with α-GFP and α-GAPDH antibodies. (B) Gpa2-GFP expression levels in glucose and 90 min raffinose treatment were quantified from immunoblots (A) using imageJ and normalized to GAPDH signal. * indicates unpaired t test ($p = 0.0287$). (C) Wild-type cells expressing endogenously expressed Gpa2-GFP were imaged by Airyscan in glucose (left) and following 2 h raffinose treatment (right) presented as max-intensity projections from four z-stack slices from center-focused cells Arrows showing vacuole (V; yellow) and cytoplasm (C; white) are shown. (D) Mean-intensity measurements for vacuole, cytoplasm, and surface from cells in (C) were performed. (E) Max-intensity

find that PI3K mutants are also defective in recycling (Figure 4). In addition to the role of PI3K in vacuolar trafficking of proteins through the biosynthetic (Robinson *et al.*, 1988; Schu *et al.*, 1993) and autophagy (Kihara *et al.*, 2001; Wurmser and Emr, 2002) pathways, Vps34 generation of PtdIns3P is required for retrograde transport (Burda *et al.*, 2002) and for the trafficking of proteins internalized from the PM and trafficked through the MVB pathway (Munn and Riezman, 1994; Katzmann, 2003). Our attempts to recover *vps15Δ* and *vps34Δ* cells from the Matα collection, or to generate the mutants by homologous recombination, were unsuccessful. Localization of the endogenously expressed Ste3-GFP-DUb reporter, which is mating type–specific, was therefore not possible. Instead, we performed experiments with Mata *vps15Δ* and *vps34Δ* mutants that are both extremely defective in FM4-64 recycling (Figure 4A), which one might reasonably expect following such dramatic abrogation of the endolysosomal system. However, our additional work suggests that the recycling pathway is modulated in response to more subtle PI3K regulatory effects. For example, we took advantage of an optimized hyperactive Vps34 allele (Vps34EDC) that stimulates overproduction of PtdIns3P, which had previously been shown to upregulate retrograde trafficking, perturb late stages of autophagy, and have no effect of MVB sorting (Steinfeld *et al.*, 2021). Expression of hyperactive Vps34 resulted in defects in FM4-64 recycling (Figure 4D), suggesting, like the late stages of autophagy, that recycling to the surface requires specific PtdIns3P regulation. This result also implies that Gpa1-PI3K–mediated recycling is distinct from retrograde trafficking routes via the Golgi (Ma *et al.*, 2017; Best *et al.*, 2020). The finding that a single point mutation in Vps15, which disrupts the interaction of the Gpa1 effector with PI3K (Heenan *et al.*, 2009), was sufficient to attenuate recycling to a similar degree as *GPA1* deletion (Figure 4, F–H) suggests that the recycling defects of *gpa1Δ* cells could be explained by improper PtdIns3P production. We note that disruption of these regulators does not exhibit the extreme FM4-64 recycling defects found in glucose-starved (Figure 1D) or PI3K-null (Figure 4C) cells, but it is similar to deletion of other factors previously shown to

projections of 3D confocal images of four z-stack slices covering the top-focused area of the cell. (F) Cells exhibiting surface puncta of Gpa2-GFP were quantified as a percentage of total population. * indicates unpaired -test ($p < 0.0001$). Scale bar, 5 μm.
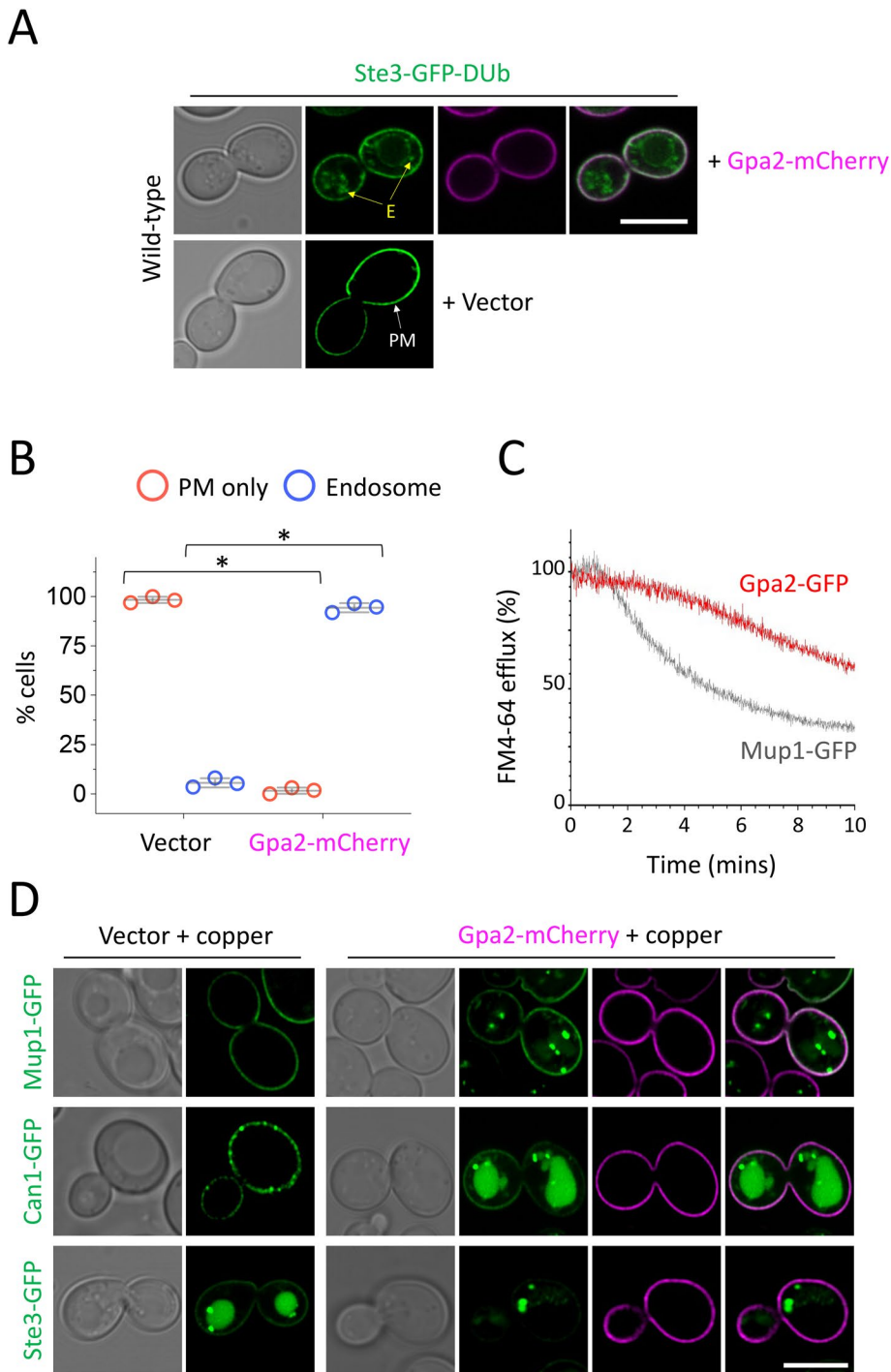
FIGURE 9: Overexpression of Gpa1 perturbs surface recycling. (A) Confocal microscopy of wild-type cells expressing Ste3-GFP-DUb with and without Gpa2-mCherry. (B) Localization of Ste3-GFP-DUb in wild-type cells transformed with vector or Gpa2-mCherry at mid–log phase was quantified from >35 cells ($n = 3$). Unpaired Student's t tests were performed, with asterisk (*) indicating $p < 0.000001$. (C) FM4-64 efflux assay was measured from wild-type cells expressing either Gpa2-GFP or Mup1-GFP. Cells were loaded with rich media containing 40 µM FM4-64 for 8 min before washing and dye efflux measured over time by flow cytometry and expressed a % of the initial 10 s fluorescence. (D) Wild-type cells expressing the copper-inducible Gpa2-mCherry construct, using 50 µM copper chloride, and coexpressing either Mup1-GFP, Can1-GFP, or Ste3-GFP were imaged using confocal microscopy. Scale bar, 5 µm.

perturb recycling, such as Rcy1, the Rag GTPases, and the Rpd3 complex (Wiederkehr *et al.*, 2000; MacDonald and Piper, 2017; Amoiradaki *et al.*, 2021). A potential connection between recycling

defects observed during glucose starvation and PI3K-Gpa1 regulation was noted due to a constitutively active Gpa1^{Q323L} mutant also being defective in recycling (Figure 5). The screen that discovered that signaling of Gpa1^{Q323L} requires PI3K also revealed that *reg1Δ* cells, which lack the phosphatase subunit Reg1 (Tu and Carlson, 1995; Sanz *et al.*, 2000), gave the largest defect in signaling across all ~5000 mutants tested (Slessareva *et al.*, 2006). Although Gpa1 phosphorylation status is controlled by glucose-associated enzymes (Elm1, Sak1, Tos3, and Glc7-Reg1), this has little impact on GDP or GTP binding (Clement *et al.*, 2013), the latter being required for PI3K-mediated production of PtdIns3P (Slessareva *et al.*, 2006). Therefore, we hypothesized that *reg1Δ* cells suppress constitutively active Gpa1 through a glucose-sensitive transcriptional response mediated via Glc7 and the downstream transcriptional repressor Mig1 (DeVit and Johnston, 1999; Shashkova *et al.*, 2017).

In support of this hypothesis, we observe recycling defects in both *reg1Δ* mutants (Figure 5, E and F) but also in *mig1Δ mig2Δ* cells (Figure 7C) lacking downstream transcriptional repressor activity (Schüller, 2003). This suggested that expression of an unknown inhibitor of Gpa1-mediated recycling would be derepressed following glucose starvation or in *mig1Δ mig2Δ* mutants. The other yeast Gα subunit, Gpa2, was the only candidate recycling inhibitor that both physically interacts with Gpa1 (Ho *et al.*, 2002) but has also been proposed as a gene product repressed by Mig1 (Wollman *et al.*, 2017). We confirmed that *GPA2* meets these criteria by being transcriptionally upregulated ~6.4 ± 0.7-fold following 1-h raffinose exchange compared with glucose-grown cells and increasing ~2.0 ± 0.3-fold in *mig1Δ mig2Δ* cells compared with wild type (Figure 7E). We went on to show that Gpa2 overexpression is sufficient to reduce recycling efficiency of Ste3-GFP-DUb, FM4-64, and various fluorescently tagged surface cargoes (Figure 9). The finding that Ste3-GFP-DUb recycling defects in *mig1Δ mig2Δ* can be suppressed by further deletion of *GPA2* supports the notion that Gpa2 is a recycling inhibitor controlled at the transcriptional level via Mig1 in response to glucose starvation (Figure 7G). The exact mechanisms of recycling inhibition via Gpa2 are not known, but we found little evidence of Gpa2 localizing to endosomal structures that might suggest a direct role with Gpa1-PI3K (Figure 10, A–E). Instead, on the basis of the increased protein levels that concentrate at the surface during glucose starvation (Figure 8) and physical interaction of Gpa1 and Gpa2 (Figure 10, F and G), we propose that elevated levels of
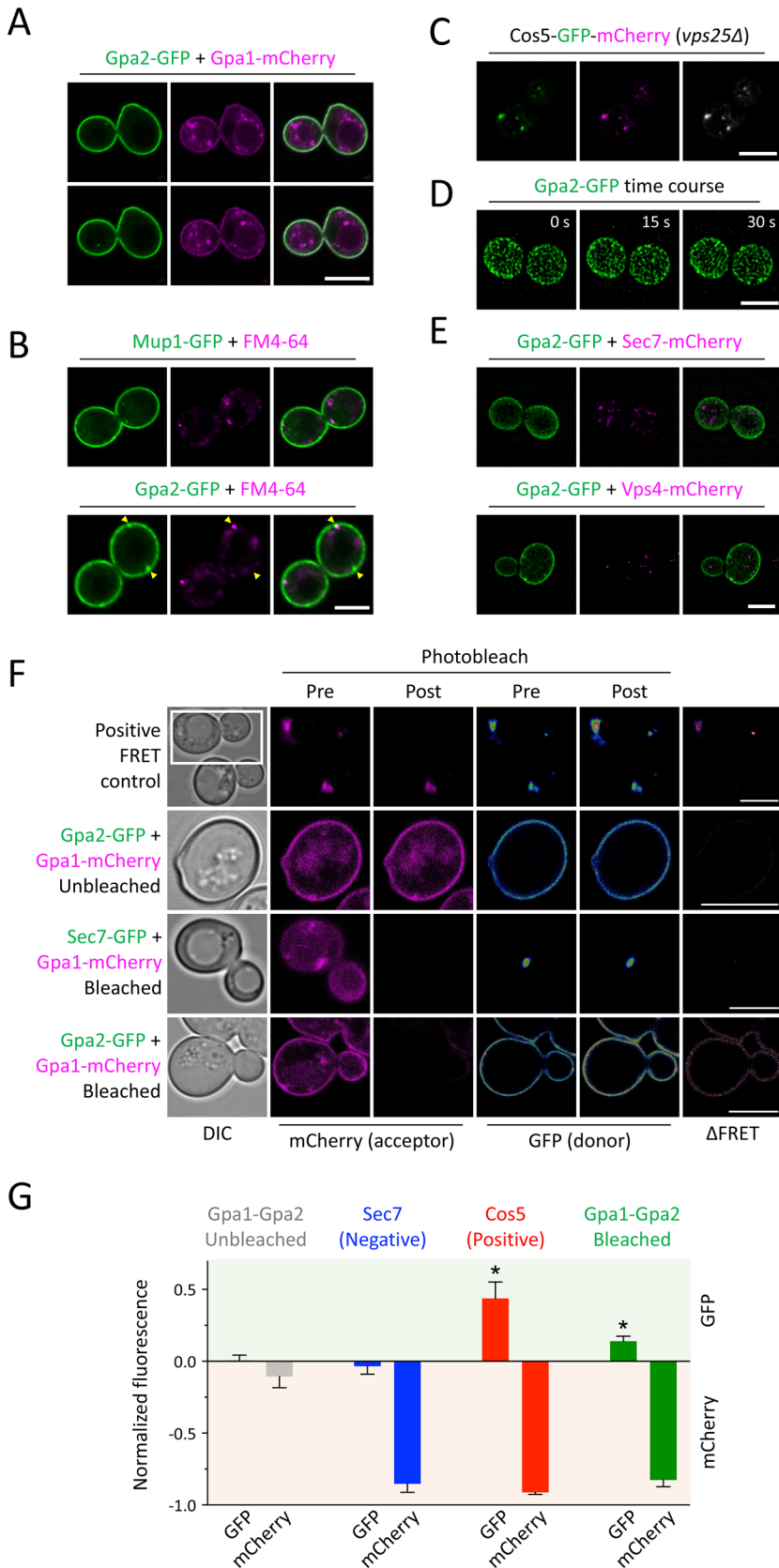
FIGURE 10: Gpa2 chiefly localizes to the PM, where it interacts with Gpa1. (A) Wild-type cells coexpressing Gpa2-GFP and Gpa1-mCherry were imaged by confocal microscopy. (B) Cells expressing either Mup1-GFP or Gpa2-GFP were labeled with 40 µM FM4-64 for 3 min followed by quenching of extracellular dye with 2.4 µM SCAS and confocal imaging. (C) 4D Apotome SIM experiments were performed for

surface localized Gpa2 following glucose starvation divert Gpa1 from endosomes, thereby attenuating PI3K activity and recycling (Figure 6B). Although our steady state evidence is not sufficient to conclude that Gpa1 is sequestered by Gpa2 at the surface, we did find an increase of surface localized Gpa1 in the recycling mutant *rcy1Δ*, suggesting at least that the distribution between surface and endosomal Gpa1 can be modulated in response to recycling efficiency (Supplemental Figure S3). Alternatively, as Gpa1 is both palymitoylated and myristoylated (Song and Dohlman, 1996; Song *et al.*, 1996), its ability to regulate endosomal lipids with PI3K may be required for its correct localization. To test our model that elevated surface levels of Gpa2 inhibit recycling by reducing PI3K production of PtdIns3P, we examined the localization of two proteins that bind endosomal membranes enriched in PtdIns3P. We found that localization of both the PX-domain protein Snx41 (Hettema *et al.*, 2003) and the FYVE-domain protein Pib1 (Shin *et al.*, 2001) were disrupted following glucose starvation, with marked reduction in membrane association (Figure 11). Support for our model that Gpa1 mediated PI3K activity is inhibited by the Gpa2 inhibitor comes from our discovery that simply overexpressing Gpa2 on a plasmid mimics glucose starvation and mislocalizes Snx41 and Pib1.

We believe that the mechanism described here serves as a medium-term transcriptional-based solution in the initial hours of starvation. As surface proteome effects are also observed more rapidly, this response presumably integrates with faster-acting regulation, potentially involving posttranslational modification of Rsp5 adaptors (Kahlhofer *et al.*, 2021), and contributes to sustained accumulation in

vps25Δ cells expressing a dual GFP- mCherry–tagged Cos5. (D) 3D time-lapse Apotome SIM microscopy was used to image wild-type cells expressing Gpa2-GFP with 42 z-stack slices to cover fluorescence across depth of cells. Maximum projections of the top 10 z-slices are shown for top-focused, surface-labeled signal. (E) Imaging was performed as described in D for wild-type cells coexpressing Gpa2-GFP with either Sec7-mCherry (top) or Vps4-mCherry (bottom), with maximum-intensity projections generated across all 42 z-stack slices for each sample shown. (F) Acceptor bleaching experiments using the 561 nm laser at 100% were performed with the expressed fluorescent proteins indicated. Conditions were optimized using a positive control: *vps25Δ* cells expressing Cos5-mCherry-GFP with a seven-amino-acid linker between mCherry and GFP designed to give maximal FRET signal (top). The Gpa2-GFP and Gpa1-mCherry experiment was controlled by assessing fluorescence from an unbleached sample and from colocalized Gpa1-mCherry and Sec7-GFP. GFP fluorescence pre- and postbleach are shown in RGB LUT format, The GFP fluorescence of prebleach was subtracted from postbleach image (ΔFRET) and the Fire LUT applied. G) Normalized fluorescence for GFP and mCherry pre- and post-bleach data sets from F were quantified from $n = 3$ experiments. * indicates $p < 0.001$; Scale bar, 5 µm.
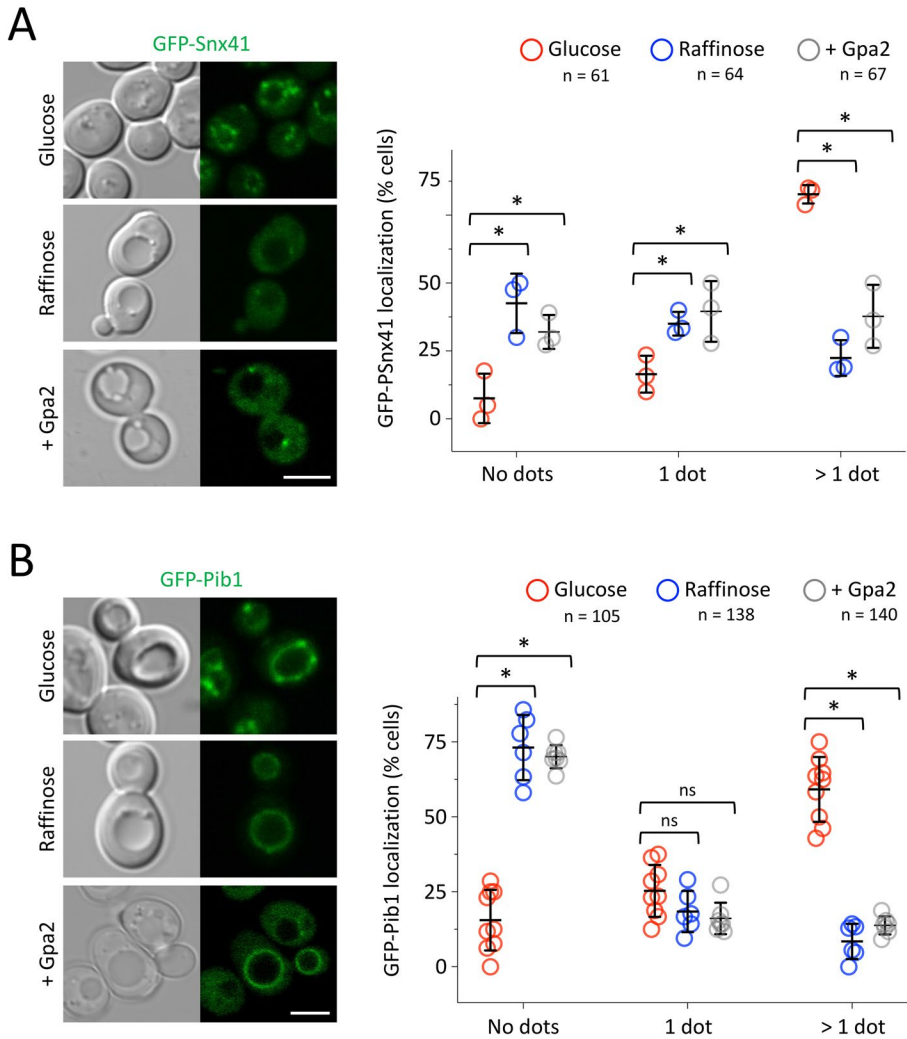
FIGURE 11: Glucose starvation and Gpa2 overexpression. (A, B) Wild-type cells expressing GFP-Snx41 (A) and GFP-Pib1 (B) were imaged in glucose-replete media, following 2 h raffinose exchange, and in cells overexpressing Gpa2. Quantifications for each experiment were performed (right) by comparing the distribution of GFP-Snx41 and GFP-Pib1 dots in each cell as a percentage. Unpaired Student's t tests were performed, with asterisk (*) indicating $p < 0.001$. Scale bar, 5 μm.

Glc7-Reg1 > Mig1 > *GPA2* pathway to modulate the surface proteome to suit nutritional availability, increase lysosomal/vacuolar degradation, and calibrate metabolic processes for cellular survival. G-protein regulators and PI3K orthologues are evolutionarily conserved (Pierce *et al.*, 2002; Engelman *et al.*, 2006), and although G-protein signaling is much more complex in animal cells, Gαs have been shown to regulate endosomal trafficking and surface protein function (Colombo *et al.*, 1992, 1994; Beron *et al.*, 1995; Zheng *et al.*, 2004; Beas *et al.*, 2012). Therefore, this mode of surface protein regulation in response to nutrition may be conserved in mammalian cells.

MATERIALS AND METHODS
Request a protocol through *Bio-protocol*.

Reagents
Supplemental tables are included to document use of yeast strains (Supplemental Table S1), plasmids (Supplemental Table S2), and statistical tests (Supplemental Table S3).

Cell culture
Yeast cells were cultured in either rich media (yeast extract peptone dextrose [YPD]; 2% glucose, 2% peptone, 1% yeast extract) or synthetic complete minimal medium (SC; 2% glucose, yeast nitrogen base supplemented with amino acid/base dropout mixtures). Cultures were routinely prepared in serial dilution overnight so that they were harvested for downstream experiments from early/mid–log phase (OD_{600} = <1.0). For glucose starvation experiments, 2% glucose media was washed 3× and exchanged with either identical media lacking any carbon source (no sugar) or media of the same recipe but instead containing 2% raffinose instead of glucose. KanMX and ClonNAT strain selections were performed in rich media containing 250 µg/ml geneticin/G418 (Formedium) or 150 µg/ml Nourseothricin (Jena Bioscience), respectively. GFP and mCherry fusions of *SEC7* were created with a methotrexate cassette selected on 20 mM methotrexate (Alfa Aesar) supplemented with 5 mg/ml sulfanilamide. The *loxP* flanked cassette was then excised by *TEF1*-Cre expression and plasmid removal, as described (MacDonald and Piper, 2015). Expression of plasmids from the *CUP1* promoter in appropriate selective media was induced by the addition of copper chloride (typically 20–100 µM).

Confocal microscopy and FRET
Cells were typically harvested from mid–log phase SC minimal media cultures and prepared for confocal microscopy on Zeiss laser scanning confocal instruments (LSM710 or LSM880 equipped with an Airyscan) using a Plan-Apochromat 63×/1.4 differential interference contrast (DIC) objective lens. The fluorescent proteins GFP, mGFP, and mNeonGreen were excited using the 488 nm line from

the vacuole over longer periods (Lang *et al.*, 2014; Müller *et al.*, 2015). Beyond the exact mechanism of Gpa2 inhibition, other important questions remain, such as the molecular function of Gpr1 and Ras2, which we confirmed are required for recycling (Figure 2C) while also being functionally associated with Gpa2 and glucose metabolism (Colombo *et al.*, 1998, 2004). We speculate that recycling inhibition via increased *GPA2* expression is distinct from its role with Gpr1-Ras to induce cAMP signaling (Xue *et al.*, 1998; Kraakman *et al.*, 1999), as overexpression of Gpa2 does not inhibit Gpr1 function; instead it triggers increased Ras signaling and cAMP accumulation (Nakafuku *et al.*, 1988). Our model would suggest that clathrin-mediated endocytosis of surface cargoes is counterbalanced by efficient Gpa1-PI3K recycling in glucose-replete conditions. In glucose, the tunable inhibitor of recycling Gpa2 is transcriptionally repressed, collectively maintaining high levels of surface proteins at the PM for optimal growth (Figure 6A). Upon glucose depletion, the Mig1-dependent increase in endocytosis via yeast AP180 adaptors (Laidlaw *et al.*, 2020) would complement decreased recycling via the

an argon laser their emission collected from 495 to 550 nm. Fluorescent protein mCherry and dye FM4-64 were excited using the 561 nm line from a yellow DPSS laser and the emission collected from 570 to 620 nm. Acceptor bleaching was used to determine the occurrence of FRET. The targeted bleaching of the mCherry (acceptor) using the 561 nm laser was used to dequench any FRET GFP (donor). Bleach acquisition was controlled by the Zeiss Zen FRAP module where a short time-lapse series was taken before and after the bleaching of mCherry. The change in GFP intensity was measured and the data exported for visual representation in Fiji or plotted as graphs in GraphPad Prism (v9.0.2).

Apotome SIM
Cells were imaged on a Zeiss Elyra 7 system using a Plan-Apochromat 40×/1.4 oil objective lens. Multicolored acquisition was performed sequentially to minimize cross-talk between channels. The fluorescent images were capture on two PCO Edge sCMOS cameras attached to a DuoLink motorized dual camera adapter and the color split using the secondary beam splitter BP420-480 + BP470-640 + LP740. The fluorescent protein mCherry was excited using the 561 nm laser line and emission collected from 570 to 640 nm. The fluorescent protein GFP was excited using the 488 nm laser line and emission collected from 490 to 570 nm. Apotome acquisition was set to collect five phase images with 25 ms camera exposure time. Yeast cells were optical Z sections using step size optimized for "Leap" acquisition. For time-lapse experiments z stacks were collected with an interval of 4.3 s. Apotome phase images were processed using Zeiss Zen Black software set to 3D SIM Leap. The alignment between the color channels was further improved by taking a Z stack of multicolor TetraSpec microspheres (ThermoFisher) that was used to generate an alignment matrix using the "Channel alignment" tool in Zen Black and applied to the time-lapse data.

Image analysis
Micrographs were processed by Zeiss Zen and Fiji software. Images were processed using Zen software (Zeiss) and were further modified (e.g., colored, merged) using Fiji.

Halo mating assay
Mata wild-type cells and *gpa1Δ* mutants transformed with either empty vector or Gpa1-mCherry cells were grown to saturation overnight, diluted in fresh SC media, and grown for ~6 h. Equal amounts of cells were estimated by measuring the OD_{600} of the culture, harvested and resuspended in 50 µl sterile water before spotting onto lawns of Matα *bar1-1* mutant cells. Lawns were created from mid–log phase cultures spread on YPD solid agar and left to dry for several hours. Plates were incubated at 30°C for 2 d before the area of growth inhibition was measured using ImageJ (National Institutes of Health) for each spot of Mata cells. These area measurements were normalized to wild-type cells from the same plate and the average plotted for four biological replicates.

Yeast RNA extraction
For gene expression analysis following glucose starvation, wild-type cells were grown to mid–log phase in YPD before being split and incubated in 10 ml YPD (dextrose) or 10 ml YPR (raffinose) media for 1 h before harvesting. For experiments to test the role of Mig1/Mig2, wild-type and *mig1Δ mig2Δ* cells were grown to mid–log phase in 10 ml YPD before harvesting. Spheroplasting of harvested yeast cells was performed for 2 min in lysis buffer (1 M sorbitol 100 mM EDTA, 0.1% β-mercaptoethanol) containing 25 U of zymolase (Zymo Research). RNA extraction was performed with an RNeasy kit

(QIAGEN) including additional DNaseI treatment using a TURBO DNA-free kit (Invitrogen).

Quantitative reverse transcription PCR (RT-qPCR)
cDNA was synthesized from 5 µg extracted RNA with SuperScript IV reverse transcriptase (Invitrogen) using 50 ng/µl random hexamers and 10 mM dNTPs. Five-minute incubations at 65°C were carried out before 100 mM dithiothreitol and ribonuclease inhibitor were added and the Superscript IV reverse transcriptase to initiate the qPCR (10 min 23°C; 10 min 55°C; 10 min 80°C) immediately. To amplify *GPA1*, oligonucleotides 361 (5' ACATCGGCTCGTCCAAATTC) and 362 (5' TCTGGTCGTATTCACTCATTGC) were used. To amplify *GPA2* oligonucleotides 365 (5' CAATGGGCCTAACGCATCG) and 366 (5' GGGTCTGTAATTGGGCGAAG) were used. All experiments were compared with the *ACT1* reference gene amplified by oligonucleotides 207 (5' CTCCACCACTGCTGAAAGAG) and 208 (5' GCAGCGGTTTGCATTTCTTG). Single product amplification was confirmed by PCR using genomic DNA as a template, and near-100% amplification efficiencies were confirmed (102.2 ± 0.12% for *GPA1*, 101.5 ± 0.03% for *GPA2*, and 100.6 ± 0.08% for *ACT1*) by duplicate qPCRs on a standard curve of known input quantity. qPCRs were performed on 20 ng cDNA, including relevant negative controls, in 20 µl reactions containing 350 nM of each primer and 10 µl Fast SYBR Green Master Mix (ThermoFisher Scientific). The QuantStudio 3 system (ThermoFisher) was used for reactions under the following conditions: 40 cycles of 95°C for 1 s, 20 s 60°C, before a continuous ramp from 60°C to 95°C at a rate of 0.1°C/s for melt curve analysis. Expression of *GPA1* and *GPA2* under the indicated conditions was quantified using the comparative Ct (ΔΔCt) method, relative to the expression of the housekeeping gene *ACT1*, and normalized to control sample (glucose for raffinose comparisons and wild-type cells for comparison with *mig1Δ mig2Δ* mutants).

Yeast genomic DNA extractions
Yeast for genotyping and genome sequencing was grown to mid–log phase in YPD before being harvested and resuspended in 50 mM Tris-HCl, 20 mM EDTA, and then 3 µl β-mercaptoethanol, 10 µl zymolyase, and 1 mg/µl RNase (QIAGEN). This was incubated in a 37°C shaker for 1 h before the addition of proteinase K (10 µl; QIAGEN; >600 mAU/ml) and left at 55°C for 1 h. Phenol:chloroform:isoamyl alcohol (500 µl) was added, and the solution was vortexed for 5 min before being spun at 15,000 rpm for 5 min. The aqueous layer was transferred to a fresh Eppendorf tube, and this was repeated two more times. The final aqueous layer was transferred to a fresh Eppendorf tube, and 50 µl of 3 M sodium acetate was added. DNA was precipitated by the addition of 1 ml 100% ethanol and spinning (10°C, 15,000 rpm) for 10 min. The pellet was then washed with 70% ethanol before residual ethanol was removed. The pellet was then dissolved in 100 µl TE Lite and left to resuspend overnight at room temperature.

Yeast genome sequencing
Before sequencing library generation, genomic DNA samples extracted as above were subjected to an additional cleanup step, by binding samples with a 1.5× volume of AMPure XP beads (Beckman Coulter), washing twice with 70% ethanol, and eluting into fresh TE. Libraries were then prepared from 500 ng genomic DNA using the NEBNext Ultra II FS DNA library prep kit for Illumina (New England Biolabs), according to the manufacturer's instructions and using a 14 min, 37°C incubation for DNA fragmentation and three cycles of PCR for incorporation of unique dual indices (NEBNext multiplex oligos for Illumina) to the final libraries. Following library quantitation

and quality assessment using the Agilent Tapestation, libraries were pooled at equimolar ratios and subjected to 150-base-paired end sequencing on an Illumina NovaSeq at Novogene, Europe.

Genome alignment and variant detection

Illumina paired-end reads were quality trimmed and verified using Cutadapt v3.4 (Martin, 2011) and FastQC (Andrews, 2010), respectively, before alignment to the *Saccharomyces cerevisiae* reference strain S288C using BWAmem (Li, 2013). Any mistakes in mate pairing and duplicates were detected and removed, and read sorting was performed using samtools v1.11 (Danecek *et al.*, 2021). Resultant bam files were visually inspected in an IGV viewer (Robinson *et al.*, 2011) for verification of the modifications to the *GPA1* locus (*gpa1Δ::kanr*) in both the BY4741 Mata and BY4742 Matα strain backgrounds. The three bam files were arranged into genomic positions using samtools, and variants were identified using VarScan v2.9.3 (Koboldt *et al.*, 2009). Variants were analyzed with SnpEff (Cingolani *et al.*, 2012) for annotation of variants as well as with Variant Effect Predictor (McLaren *et al.*, 2016) for confirmation.

Flow cytometry

Fluorescence intensity of different strains stably expressing Ste3-GFP-DUb was measured using a CytoFLEX flow cytometer (Beckman Coulter) with 488 nm laser excitation, 525/40 nm emission filter, and avalanche photo diode detector. Approximately 75,000 cells in culture medium per sample were analyzed with logical gating (forward/side scatter: single cells) used to quantify GFP fluorescence-positive yeast cells. Sample analysis was performed using the software FCS Express v7.04 (DeNovo Software).

FM4-64 recycling assay

Cells were grown to mid–log phase in YPD, or SC-Ura minimal media when plasmid selection was necessary, before 1 ml of cells (OD = 1.0) was harvested and incubated in 100 µl YPD containing 40 µM FM4-64 dye (*N*-(3-triethylammoniumpropyl)-4-(6-(4-(diethylamino) phenyl)hexatrienyl)pyridinium dibromide) dye for 8 min at room temperature. Cells were then washed 3× in cold SC media, with each wash left for 3 min on ice, before the final wash was concentrated in 100 µl SC media in preparation for flow cytometry. For raffinose and glucose starvation media, the same rich and SC media was used with glucose exchanged with either no sugar or 2% raffinose. Concentrated cells (20 µl) were brought up in 3 ml room temperature SC medium and approximately analyzed by flow cytometry at 1000–2500 cells per second using an LSR Fortessa X20 instrument (BD Biosciences). FM4-64 intensity was measured over a 10-min period with 561 nm laser excitation and emission filter 710/50. Measurements from 488 nm laser excitation with 530/50 nm emission filter were also recorded for monitoring background autofluorescence. Any comparisons are performed from cells labeled at the same time in the same media, with empty vector controls included when effects from plasmids are to be assessed.

Image quantification for Mig1-GFP

The nuclear signal of Mig1-GFP was calculated as a percentage of nuclear/total signal in the green channel, as shown in Supplemental Figure S2. Briefly, whole cells were segmented based on a DIC image using the Cell Magic Wand plug-in (Min = 8, Max = 300, roughness = 2.0) and used to calculate the total (nuclear plus cytoplasmic) signal for each cell in the Mig1-GFP/Green channel. The Nrd1-mCherry signal was used with *otsu* threshold to segment the nucleus based on the red channel, and these regions of interest were applied to measure nuclear Mig1-GFP from the green channel.

Statistical analyses

Unpaired Student's *t* tests were performed using GraphPad Prism v8.3.1. to compare the statistical significance between experimental conditions, with an asterisk (*) used to denote *p* values of <0.05 or less, as mentioned in specific figure legends, or (ns) used to define differences that are not significant.

REFERENCES

Amoiradaki K, Bunting KR, Paine KM, Ayre JE, Hogg K, Laidlaw KME, MacDonald C (2021). The Rpd3-complex regulates expression of multiple cell surface recycling factors in yeast. Int J Mol Sci 22, 12477.

Andrews S (2010). FastQC: A quality control tool for high throughput sequence data. http://www.bioinformatics.babraham.ac.uk/projects/fastqc/.

Apanovitch DM, Slep KC, Sigler PB, Dohlman HG (1998). Sst2 is a GTPase-activating protein for Gpa1: purification and characterization of a cognate RGS–Gα protein pair in yeast. Biochemistry 37, 4815–4822.

Babst M, Katzmann DJ, Estepa-Sabal EJ, Meerloo T, Emr SD (2002a). Escrt-III: an endosome-associated heterooligomeric protein complex required for mvb sorting. Dev Cell 3, 271–282.

Babst M, Katzmann DJ, Snyder WB, Wendland B, Emr SD (2002b). Endosome-associated complex, ESCRT-II, recruits transport machinery for protein sorting at the multivesicular body. Dev Cell 3, 283–289.

Beas AO, Taupin V, Teodorof C, Nguyen LT, Garcia-Marcos M, Farquhar MG (2012). Gαs promotes EEA1 endosome maturation and shuts down proliferative signaling through interaction with GIV (Girdin). Mol Biol Cell 23, 4623–4634.

Beron W, Colombo MI, Mayorga LS, Stahl PD (1995). In vitro reconstitution of phagosome-endosome fusion: evidence for regulation by heterotrimeric Gtpases. Arch Biochem Biophys 317, 337–342.

Best JT, Xu P, McGuire JG, Leahy SN, Graham TR (2020). Yeast synaptobrevin, Snc1, engages distinct routes of postendocytic recycling mediated by a sorting nexin, Rcy1-COPI, and retromer. Mol Biol Cell 31, 944–962.

Binda M, Péli-Gulli M-P, Bonfils G, Panchaud N, Urban J, Sturgill TW, Loewith R, Virgilio CD (2009). The Vam6 GEF controls TORC1 by activating the EGO complex. Mol Cell 35, 563–573.

Blumer KJ, Thorner J (1990). Beta and gamma subunits of a yeast guanine nucleotide-binding protein are not essential for membrane association of the alpha subunit but are required for receptor coupling. Proc Natl Acad Sci USA 87, 4363–4367.

Bonfils G, Jaquenoud M, Bontron S, Ostrowicz C, Ungermann C, Virgilio CD (2012). Leucyl-tRNA synthetase controls TORC1 via the EGO complex. Mol Cell 46, 105–110.

Broggi S, Martegani E, Colombo S (2013). Live-cell imaging of endogenous Ras-GTP shows predominant Ras activation at the plasma membrane and in the nucleus in Saccharomyces cerevisiae. Int J Biochem Cell Biol 45, 384–394.

Buelto D, Hung C, Aoh QL, Lahiri S, Duncan MC (2020). Plasma membrane to vacuole traffic induced by glucose starvation requires Gga2-dependent sorting at the trans-Golgi network. Biol Cell 112, 349–367.

Burd CG, Emr SD (1998). Phosphatidylinositol(3)-phosphate signaling mediated by specific binding to RING FYVE domains. Mol Cell 2, 157–162.

Burda P, Padilla SM, Sarkar S, Emr SD (2002). Retromer function in endosome-to-Golgi retrograde transport is regulated by the yeast Vps34 PtdIns 3-kinase. J Cell Sci 115, 3889–3900.

Camilli PD, Emr SD, McPherson PS, Novick P (1996). Phosphoinositides as regulators in membrane traffic. Science 271, 1533–1539.

Chen K, Healy MD, Collins BM (2019). Towards a molecular understanding of endosomal trafficking by Retromer and Retriever. Traffic 20, 465–478.

Cingolani P, Platts A, Wang LL, Coon M, Nguyen T, Wang L, Land SJ, Lu X, Ruden DM (2012). A program for annotating and predicting the effects of single nucleotide polymorphisms, SnpEff. Fly 6, 80–92.

Clement ST, Dixit G, Dohlman HG (2013). Regulation of yeast G protein signaling by the kinases that activate the AMPK homolog Snf1. Sci Signal 6, ra78.

Colombo M, Mayorga L, Casey P, Stahl P (1992). Evidence of a role for heterotrimeric GTP-binding proteins in endosome fusion. Science 255, 1695–1697.

Colombo MI, Mayorga LS, Nishimoto I, Ross EM, Stahl PD (1994). Gs regulation of endosome fusion suggests a role for signal transduction pathways in endocytosis. J Biol Chem 269, 14919–14923.

Colombo S, Ma P, Cauwenberg L, Winderickx J, Crauwels M, Teunissen A, Nauwelaers D, de Winde JH, Gorwa M, Colavizza D, et al. (1998). Involvement of distinct G-proteins, Gpa2 and Ras, in glucose- and intra-cellular acidification-induced cAMP signalling in the yeast Saccharomyces cerevisiae. EMBO J 17, 3326–3341.

Colombo S, Ronchetti D, Thevelein JM, Winderickx J, Martegani E (2004). Activation state of the Ras2 protein and glucose-induced signaling in Saccharomyces cerevisiae. J Biol Chem 279, 46715–46722.

Danecek P, Bonfield JK, Liddle J, Marshall J, Ohan V, Pollard MO, Whitwham A, Keane T, McCarthy SA, Davies RM, et al. (2021). Twelve years of SAMtools and BCFtools. Gigascience 10, giab008.

de la Fuente G, Sols A (1962). Transport of sugars in yeasts II. Mechanisms of utilization of disaccharides and related glycosides. Biochim Biophys Acta 56, 49–62.

DeVit MJ, Johnston M (1999). The nuclear exportin Msn5 is required for nuclear export of the Mig1 glucose repressor of Saccharomyces cerevisiae. Curr Biol 9, 1231–1241.

Dietzel C, Kurjan J (1987). The yeast SCG1 gene: a Gα-like protein impli-cated in the a- and α-factor response pathway. Cell 50, 1001–1010.

Dixit G, Baker R, Sacks CM, Torres MP, Dohlman HG (2014). Guanine nucleotide-binding protein (Gα) endocytosis by a cascade of ubiquitin binding domain proteins is required for sustained morphogenesis and proper mating in yeast. J Biol Chem 289, 15052–15063.

Dohlman HG, Song J, Ma D, Courchesne WE, Thorner J (1996). Sst2, a negative regulator of pheromone signaling in the yeast Saccharomyces cerevisiae: expression, localization, and genetic interaction and physical association with Gpa1 (the G-protein alpha subunit). Mol Cell Biol 16, 5194–5209.

Engelman JA, Luo J, Cantley LC (2006). The evolution of phosphatidylino-sitol 3-kinases as regulators of growth and metabolism. Nat Rev Genet 7, 606–619.

Finicle BT, Jayashankar V, Edinger AL (2018). Nutrient scavenging in cancer. Nat Rev Cancer 18, 619–633.

Heenan EJ, Vanhooke JL, Temple BR, Betts L, Sondek JE, Dohlman HG (2009). Structure and function of Vps15 in the endosomal G protein signaling pathway. Biochemistry 48, 6390–6401.

Herman PK, Emr SD (1990). Characterization of VPS34, a gene required for vacuolar protein sorting and vacuole segregation in Saccharomyces cerevisiae. Mol Cell Biol 10, 6742–6754.

Hettema EH, Lewis MJ, Black MW, Pelham HRB (2003). Retromer and the sorting nexins Snx4/41/42 mediate distinct retrieval pathways from yeast endosomes. EMBO J 22, 548–557.

Ho Y, Gruhler A, Heilbut A, Bader GD, Moore L, Adams SL, Millar A, Taylor P, Bennett K, Boutilier K, et al. (2002). Systematic identification of protein complexes in Saccharomyces cerevisiae by mass spectrometry. Nature 415, 180–183.

Hong S-P, Leiper FC, Woods A, Carling D, Carlson M (2003). Activation of yeast Snf1 and mammalian AMP-activated protein kinase by upstream kinases. Proc Natl Acad Sci USA 100, 8839–8843.

Johnston M, Flick JS, Pexton T (1994). Multiple mechanisms provide rapid and stringent glucose repression of GAL gene expression in Saccharomyces cerevisiae. Mol Cell Biol 14, 3834–3841.

Kahlhofer J, Leon S, Teis D, Schmidt O (2021). The α-arrestin family of ubiquitin ligase adaptors links metabolism with selective endocytosis. Biol Cell 113, 183–219.

Katzmann DJ (2003). Vps27 recruits ESCRT machinery to endosomes during MVB sorting. J Cell Biol 162, 413–423.

Katzmann DJ, Babst M, Emr SD (2001). Ubiquitin-dependent sorting into the multivesicular body pathway requires the function of a conserved endosomal protein sorting complex, ESCRT-I. Cell 106, 145–155.

Kihara A, Noda T, Ishihara N, Ohsumi Y (2001). Two distinct Vps34 phospha-tidylinositol 3–kinase complexes function in autophagy and carboxypep-tidase Y sorting in Saccharomyces cerevisiae. J Cell Biol 152, 519–530.

Koboldt DC, Chen K, Wylie T, Larson DE, McLellan MD, Mardis ER, Weinstock GM, Wilson RK, Ding L (2009). VarScan: variant detection in massively parallel sequencing of individual and pooled samples. Bioin-formatics 25, 2283–2285.

Kraakman L, Lemaire K, Ma P, Teunissen A, Donaton MCV, Dijck PV, Wind-erickx J, Winde JHD, Thevelein JM (1999). A Saccharomyces cerevisiae G-protein coupled receptor, Gpr1, is specifically required for glucose activation of the cAMP pathway during the transition to growth on glucose. Mol Microbiol 32, 1002–1012.

Laidlaw KME, Calder G, MacDonald C (2021). Recycling of nutrient transporters from yeast endosomes is regulated by ubiquitinated Ist1. bioRxiv, https://doi.org/10.1101/2021.06.19.449106.

Laidlaw KME, Bisinski DD, Shashkova S, Paine KM, Veillon MA, Leake MC, MacDonald C (2020). A glucose-starvation response governs endocytic trafficking and eisosomal retention of surface cargoes in budding yeast. J Cell Sci 134, jcs257733.

Laidlaw KME, MacDonald C (2018). Endosomal trafficking of yeast mem-brane proteins. Biochem Soc Trans 46, 1551–1558.

Lang MJ, Martinez-Marquez JY, Prosser DC, Ganser LR, Buelto D, Wendland B, Duncan MC (2014). Glucose starvation inhibits autophagy via vacu-olar hydrolysis and induces plasma membrane internalization by down-regulating recycling. J Biol Chem 289, 16736–16747.

Li H (2013). Aligning sequence reads, clone sequences and assembly con-tigs with BWA-MEM. Arxiv, 1303.3997v2.

Li M, Koshi T, Emr SD (2015). Membrane-anchored ubiquitin ligase complex is required for the turnover of lysosomal membrane proteins. J Cell Biol 211, 639–652.

Lindmo K, Stenmark H (2006). Regulation of membrane traffic by phos-phoinositide 3-kinases. J Cell Sci 119, 605–614.

Ludin K, Jiang R, Carlson M (1998). Glucose-regulated interaction of a regulatory subunit of protein phosphatase 1 with the Snf1 protein kinase in Saccharomyces cerevisiae. Proc Natl Acad Sci USA 95, 6245–6250.

Lundin M, Nehlin JO, Ronne H (1994). Importance of a flanking AT-rich re-gion in target site recognition by the GC box-binding zinc finger protein MIG1. Mol Cell Biol 14, 1979–1985.

Lutfiyya LL, Iyer VR, DeRisi J, DeVit MJ, Brown PO, Johnston M (1998). Characterization of three related glucose repressors and genes they regulate in Saccharomyces cerevisiae. Genetics 150, 1377–1391.

Ma M, Burd CG (2019). Retrograde trafficking and quality control of yeast synaptobrevin, Snc1, are conferred by its transmembrane domain. Mol Biol Cell 30, 1729–1742.

Ma M, Burd CG (2020). Retrograde trafficking and plasma membrane recy-cling pathways of the budding yeast Saccharomyces cerevisiae. Traffic 21, 45–59.

Ma M, Burd CG, Chi RJ (2017). Distinct complexes of yeast Snx4 family SNX-BARs mediate retrograde trafficking of Snc1 and Atg27. Traffic 18, 134–144.

MacDonald C, Buchkovich NJ, Stringer DK, Emr SD, Piper RC (2012a). Cargo ubiquitination is essential for multivesicular body intralumenal vesicle formation. EMBO Rep 13, 331–338.

MacDonald C, Payne JA, Aboian M, Smith W, Katzmann DJ, Piper RC (2015a). A family of tetraspans organizes cargo for sorting into multive-sicular bodies. Dev Cell 33, 328–342.

MacDonald C, Piper RC (2015). Puromycin- and methotrexate-resistance cassettes and optimized Cre-recombinase expression plasmids for use in yeast. Yeast 32, 423–438.

MacDonald C, Piper RC (2016). Cell surface recycling in yeast: mechanisms and machineries. Biochem Soc Trans 44, 474–478.

MacDonald C, Piper RC (2017). Genetic dissection of early endosomal recycling highlights a TORC1-independent role for Rag GTPases. J Cell Biol 8, jcb.201702177.

MacDonald C, Shields SB, Williams CA, Winistorfer S, Piper RC (2020). A cycle of ubiquitination regulates adaptor function of the Nedd4-family ubiquitin ligase Rsp5. Curr Biol 30, 465–479.e5.

MacDonald C, Stamnes MA, Katzmann DJ, Piper RC (2015b). Tetraspan cargo adaptors usher GPI-anchored proteins into multivesicular bodies. Cell Cycle 14, 3673–3678.

MacDonald C, Stringer DK, Piper RC (2012b). Sna3 is an Rsp5 adaptor protein that relies on ubiquitination for its MVB sorting. Traffic 13, 586–598.

MacDonald C, Winistorfer S, Pope RM, Wright ME, Piper RC (2017). Enzyme reversal to explore the function of yeast E3 ubiquitin-ligases. Traffic 18, 465–484.

MacGurn JA, Hsu P-C, Smolka MB, Emr SD (2011). TORC1 regulates endocytosis via Npr1-mediated phosphoinhibition of a ubiquitin ligase adaptor. Cell 147, 1104–1117.

Martin M (2011). Cutadapt removes adapter sequences from high-through-put sequencing reads. EMBnet.journal 17, 10–12.

McLaren W, Gil L, Hunt SE, Riat HS, Ritchie GRS, Thormann A, Flicek P, Cunningham F (2016). The Ensembl variant effect predictor. Genome Biol 17, 122.

Miyajima I, Nakafuku M, Nakayama N, Brenner C, Miyajima A, Kaibuchi K, Arai K, Kaziro Y, Matsumoto K (1987). GPA1, a haploid-specific essential gene, encodes a yeast homolog of mammalian G protein which may be involved in mating factor signal transduction. Cell 50, 1011–1019.

Müller M, Schmidt O, Angelova M, Faserl K, Weys S, Kremser L, Pfaffenwimmer T, Dalik T, Kraft C, Trajanoski Z, et al. (2015). The coordinated action of the MVB pathway and autophagy ensures cell survival during starvation. eLife 4, e07736.

Munn AL, Riezman H (1994). Endocytosis is required for the growth of vacuolar H(+)-ATPase-defective yeast: identification of six new END genes. J Cell Biol 127, 373–386.

Nakafuku M, Obara T, Kaibuchi K, Miyajima I, Miyajima A, Itoh H, Nakamura S, Arai K, Matsumoto K, Kaziro Y (1988). Isolation of a second yeast Saccharomyces cerevisiae gene (GPA2) coding for guanine nucleotide-binding regulatory protein: studies on its structure and possible functions. Proc Natl Acad Sci USA 85, 1374–1378.

Nakayama N, Kaziro Y, Arai K, Matsumoto K (1988). Role of STE genes in the mating factor signaling pathway mediated by GPA1 in Saccharomyces cerevisiae. Mol Cell Biol 8, 3777–3783.

Nehlin JO, Ronne H (1990). Yeast MIG1 repressor is related to the mammalian early growth response and Wilms' tumour finger proteins. EMBO J 9, 2891–2898.

O'Donnell AF, McCartney RR, Chandrashekarappa DG, Zhang BB, Thorner J, Schmidt MC (2015). 2-deoxyglucose impairs Saccharomyces cerevisiae growth by stimulating Snf1-regulated and α-arrestin-mediated trafficking of hexose transporters 1 and 3. Mol Cell Biol 35, 939–955.

O'Donnell AF, Schmidt MC (2019). AMPK-mediated regulation of alpha-arrestins and protein trafficking. Int J Mol Sci 20, 515.

Paine KM, Ecclestone GB, MacDonald C (2021). Fur4-mediated uracil-scavenging to screen for surface protein regulators. Traffic 22, 397–408.

Péli-Gulli M-P, Sardu A, Panchaud N, Raucci S, Virgilio CD (2015). Amino acids stimulate TORC1 through Lst4-Lst7, a GTPase-activating protein complex for the rag family GTPase Gtr2. Cell Rep 13, 1–7.

Pierce KL, Premont RT, Lefkowitz RJ (2002). Seven-transmembrane receptors. Nat Rev Mol Cell Biol 3, 639–650.

Reggiori F, Pelham HRB (2002). A transmembrane ubiquitin ligase required to sort membrane proteins into multivesicular bodies. Nat Cell Biol 4, 117–123.

Reidick C, Boutouja F, Platta HW (2017). The class III phosphatidylinositol 3-kinase Vps34 in Saccharomyces cerevisiae. Biol Chem 398, 677–685.

Robinson JS, Klionsky DJ, Banta LM, Emr SD (1988). Protein sorting in Saccharomyces cerevisiae: isolation of mutants defective in the delivery and processing of multiple vacuolar hydrolases. Mol Cell Biol 8, 4936–4948.

Robinson JT, Thorvaldsdóttir H, Winckler W, Guttman M, Lander ES, Getz G, Mesirov JP (2011). Integrative genomics viewer. Nat Biotechnol 29, 24–26.

Santangelo GM (2006). Glucose signaling in Saccharomyces cerevisiae. Microbiol Mol Biol Rev 70, 253–282.

Sanz P, Alms GR, Haystead TAJ, Carlson M (2000). Regulatory interactions between the Reg1-Glc7 protein phosphatase and the Snf1 protein kinase. Mol Cell Biol 20, 1321–1328.

Sardana R, Emr SD (2021). Membrane protein quality control mechanisms in the endo-lysosome system. Trends Cell Biol 31, 269–283.

Schu P, Takegawa K, Fry M, Stack J, Waterfield M, Emr S (1993). Phosphatidylinositol 3-kinase encoded by yeast VPS34 gene essential for protein sorting. Science 260, 88–91.

Schüller H-J (2003). Transcriptional control of nonfermentative metabolism in the yeast Saccharomyces cerevisiae. Curr Genet 43, 139–160.

Selwan EM, Finicle BT, Kim SM, Edinger AL (2016). Attacking the supply wagons to starve cancer cells to death. FEBS Lett 590, 885–907.

Shashkova S, Wollman AJM, Leake MC, Hohmann S (2017). The yeast Mig1 transcriptional repressor is dephosphorylated by glucose-dependent and -independent mechanisms. FEMS Microbiol Lett 364, doi: 10.1093/femsle/fnx133.

Shin ME, Ogburn KD, Varban OA, Gilbert PM, Burd CG (2001). FYVE domain targets Pib1p ubiquitin ligase to endosome and vacuolar membranes. J Biol Chem 276, 41388–41393.

Slessareva JE, Routt SM, Temple B, Bankaitis VA, Dohlman HG (2006). Activation of the phosphatidylinositol 3-kinase Vps34 by a G protein α subunit at the endosome. Cell 126, 191–203.

Song J, Dohlman HG (1996). Partial constitutive activation of pheromone responses by a palmitoylation-site mutant of a G protein α subunit in yeast. Biochemistry 35, 14806–14817.

Song J, Hirschman J, Gunn K, Dohlman HG (1996). Regulation of membrane and subunit interactions by N-myristoylation of a G protein α subunit in yeast. J Biol Chem 271, 20273–20283.

Spira F, Mueller NS, Beck G, Olshausen P, Beig J, Wedlich-Söldner R (2012). Patchwork organization of the yeast plasma membrane into numerous coexisting domains. Nat Cell Biol 14, 640.

Stack JH, Herman PK, Schu PV, Emr SD (1993). A membrane-associated complex containing the Vps15 protein kinase and the Vps34 PI 3-kinase is essential for protein sorting to the yeast lysosome-like vacuole. EMBO J 12, 2195–2204.

Steinfeld N, Lahiri V, Morrison A, Metur SP, Klionsky DJ, Weisman LS (2021). Elevating PI3P drives select downstream membrane trafficking pathways. Mol Biol Cell 32, 143–156.

Stringer DK, Piper RC (2011). A single ubiquitin is sufficient for cargo protein entry into MVBs in the absence of ESCRT ubiquitination. J Cell Biol 192, 229–242.

Thevelein JM (1994). Signal transduction in yeast. Yeast 10, 1753–1790.

Treitel MA, Kuchin S, Carlson M (1998). Snf1 protein kinase regulates phosphorylation of the Mig1 repressor in Saccharomyces cerevisiae. Mol Cell Biol 18, 6273–6280.

Tu J, Carlson M (1994). The GLC7 type 1 protein phosphatase is required for glucose repression in Saccharomyces cerevisiae. Mol Cell Biol 14, 6789–6796.

Tu J, Carlson M (1995). REG1 binds to protein phosphatase type 1 and regulates glucose repression in Saccharomyces cerevisiae. EMBO J 14, 5939–5946.

Urbanowski JL, Piper RC (2001). Ubiquitin sorts proteins into the intralumenal degradative compartment of the late-endosome/vacuole. Traffic 2, 622–630.

Vallier LG, Carlson M (1994). Synergistic release from glucose repression by mig1 and ssn mutations in Saccharomyces cerevisiae. Genetics 137, 49–54.

Vida TA, Emr SD (1995). A new vital stain for visualizing vacuolar membrane dynamics and endocytosis in yeast. J Cell Biol 128, 779–792.

Westholm JO, Nordberg N, Murén E, Ameur A, Komorowski J, Ronne H (2008). Combinatorial control of gene expression by the three yeast repressors Mig1, Mig2 and Mig3. BMC Genomics 9, 601.

Whiteway M, Hougan L, Dignard D, Thomas DY, Bell L, Saari GC, Grant FJ, O'Hara P, MacKay VL (1989). The STE4 and STE18 genes of yeast encode potential β and γ subunits of the mating factor receptor-coupled G protein. Cell 56, 467–477.

Wiederkehr A, Avaro S, Prescianotto-Baschong C, Haguenauer-Tsapis R, Riezman H (2000). The F-box protein Rcy1p is involved in endocytic membrane traffic and recycling out of an early endosome in Saccharomyces cerevisiae. J Cell Biol 149, 397–410.

Wollman AJ, Shashkova S, Hedlund EG, Friemann R, Hohmann S, Leake MC (2017). Transcription factor clusters regulate genes in eukaryotic cells. eLife 6, e27451.

Wurmser AE, Emr SD (2002). Novel PtdIns(3)P-binding protein Etf1 functions as an effector of the Vps34 PtdIns 3-kinase in autophagy. J Cell Biol 158, 761–772.

Xu P, Hankins HM, MacDonald C, Erlinger SJ, Frazier MN, Diab NS, Piper RC, Jackson LP, MacGurn JA, Graham TR (2017). COPI mediates recycling of an exocytic SNARE by recognition of a ubiquitin sorting signal. eLife 6, e28342.

Xue Y, Batlle M, Hirsch JP (1998). GPR1 encodes a putative G protein-coupled receptor that associates with the Gpa2p Gα subunit and functions in a Ras-independent pathway. EMBO J 17, 1996–2007.

Yang X, Zhang W, Wen X, Bulinski PJ, Chomchai DA, Arines FM, Liu YY, Sprenger S, Teis D, Klionsky DJ, et al. (2020). TORC1 regulates vacuole membrane composition through ubiquitin- and ESCRT-dependent microautophagy. J Cell Biol 219, e201902127.

Yu JW, Lemmon MA (2001). All phox homology (PX) domains from Saccharomyces cerevisiae specifically recognize phosphatidylinositol 3-phosphate. J Biol Chem 276, 44179–44184.

Zheng B, Lavoie C, Tang T-D, Ma P, Meerloo T, Beas A, Farquhar MG (2004). Regulation of epidermal growth factor receptor degradation by heterotrimeric Gαs protein. Mol Biol Cell 15, 5538–5550.